EXPLORATION OF AN ELECTROCHEMICAL SENSOR FOR CONTINUOUS MONITORING OF ESTRADIOL IN APPLICATION TO FERTILITY TRACKING

by

Julia Sommer Dominesey

A thesis submitted to the faculty of
The University of Utah
in partial fulfillment of the requirements for the degree of

Master of Science

Department of Mechanical Engineering

The University of Utah

May 2022

The University of Utah Graduate School

STATEMENT OF THESIS APPROVAL

The thesis of **Julia Sommer Dominesey**

has been approved by the following supervisory committee members:

Shad Roundy	, Chair	**date approved** Date Approved
Marc Porter	, Member	**date approved** Date Approved
Himanshu Sant	, Member	**date approved** Date Approved

and by **Bruce K. Gale** , Chair/Dean of

the Department/College/School of **Mechanical Engineering**

and by David B. Kieda, Dean of The Graduate School.

ABSTRACT

This thesis is an exploration into the development of an implantable, continuously-sampling electrochemical estradiol sensor for fertility tracking. Estradiol is the primary female sex hormone that fluctuates diurnally, and monthly, dictating the menstrual cycle. A sensor that allows for continuous monitoring could be used by an individual as a family planning tool or a diagnostic tool in determining fertility issues.

The development of a repeatable, reliable bench-top estradiol measuring system is the first step in the exploration of the feasibility of our sensor. We used a three-electrode system with a gold working electrode, platinum counter electrode and Ag/AgCl reference electrode to perform cyclic voltammetry. Single-stranded DNA specific to estradiol, estradiol aptamers, were immobilized on the working electrode surface. Once coated in aptamer, we exposed the working electrode to 10ng/mL, 100ng/mL and 1,000ng/mL estradiol concentrations and analyzed the resulting capacitance change. A second set of experiments tested the ability for continuous monitoring: allowing bound aptamers to sit in electrolyte and performing continual cyclic voltammetry experiments to find if and when the estradiol molecule was dissociating from the aptamer.

From our experiments, we were able to determine that the effect of the concentration of estradiol was the most significant factor in determining the resulting capacitance. The dissociation experiments were inconclusive in determining the presence or rate of dissociation; however, our theoretical work leads us to believe that the sensor's

lag would be minimal enough to provide satisfactory data for clinical use.

In its current configuration, the sensor could be used to detect the presence of estradiol in a bench-top scenario. For its intended use, the sensor's sensitivity must increase, its size must decrease, and further experimentation would need to be conducted to prove that the dissociation theory is pragmatic.

TABLE OF CONTENTS

LIST OF TABLES

Tables

LIST OF FIGURES

Figures

ACKNOWLEDGMENTS

Thank you to Dr. Marc Porter and Eamonn Clarke for their lab space, guidance, and expertise. I would also like to thank Dr. Himanshu Sant for his guidance. A special thank you to Jeanna Tachiki Ryan for her willingness to provide insight into her work with Layla Wellness and the clinical perspective. This thesis would not have been possible without the support of my thesis advisor and mentor, Dr. Shad Roundy, who believed in me enough to take on this exploratory project. Lastly, I want to thank my parents for their encouragement and unwavering dedication to me and my education throughout my life.

CHAPTER 1

INTRODUCTION AND MOTIVATION

1.1 Introduction to Project and Thesis

The intention of this thesis is to begin the development of an electrochemical sensor for the purpose of in vivo estradiol detection in context of fertility monitoring. The literature review necessary for this thesis is disseminated throughout the chapters of this thesis, rather than grouped together in the introduction, to promote continuity for the reader. Chapter one covers motivation and current fertility tracking solutions. Chapter two analyzes the specification requirements for an in vivo estradiol sensor. Chapter three and four provide the results of the experiments run for this study. Finally, chapter five contextualizes and discusses these results, in addition to providing suggesting for future work. It is important to note that while this thesis will sometimes refer to users as women/females, or define words, devices, etc., by female-gendered terms, we recognize that there are individuals who menstruate/ovulate that this work is relevant to that do not define themselves by female-gendered descriptors.

1.2 Importance of Fertility Tracking

Estradiol (E2) is the form of the estrogen female sex hormone that is primarily responsible for each step in the menstrual cycle [1]. Tracking estradiol continuously will allow users and their health care providers to know with certainty where they are in the

menstrual cycle to help time or avoid pregnancy. Additionally, continuous monitoring can serve as a diagnostic aid in determining a hormone imbalance or fertility disorder.

1.2.1 Pregnancy and Birth Control

Health care providers and ovulating individuals rely on mediocre prediction techniques to track fertility cycles. Current methods of tracking the menstrual cycle include blood testing, the calendar method, and measuring Basal body temperature [2]; all of these methods will be expanded upon in the next section. However, none of these methods track hormones directly and continuously. Given the current options, it is nearly impossible for an ovulating individual to accurately predict their menstrual cycle from home.

The aforementioned methods work on the assumption of a consistent menstrual cycle, which is often not the case [3], especially with the rise of hormonal birth control. Hormonal birth controls release estrogen and progestin to prevent ovulation from occurring. Hormonal birth controls can cause irregular cycles, preventing an individual from using their menstrual cycle as an accurate metric of their overall health [4]. Various side effects from these types of birth controls can mimic the symptoms of fertility disorders.

Therefore, the ideal fertility tracker is a sensor with the ability to track estradiol continuously. A consistent, live reading of estradiol provides accurate fertility information. Those who wish to become pregnant can use it to target certain days, and those who wish to avoid pregnancy can use it to avoid those days.

1.2.2. Hormone Imbalances

Hormone imbalances are often an indicator of serious health risks. In women, estrogen imbalances can be a symptom of osteoporosis, carcinomas, and autoimmune rheumatic diseases [5].

Osteoporosis is a porous and/or fragile bone condition that puts an individual at risk for fractures and general pain. Decreased estradiol levels are often responsible for cortical bone loss, contributing to osteoporosis [6]. Many factors must be investigated to diagnose an individual with osteoporosis: clinical history, endocrine regulation, fracture characteristics, bone mineral density, and estradiol levels [6, 7]. While tracking estradiol cannot solely determine if an individual has osteoporosis, it can be an important contribution to the patient's health profile.

An estrogen hormonal imbalance could also be associated with breast cancer. Breast cancer is the most common type of carcinoma associated with abnormal levels of estrogen due to estrogen exposure. Estrogen plays a role both in the inception and potential detection of cancers. Estrogens can induce rapid proliferation of breast epithelial cells; rapid proliferation makes cells prone to genetic errors which can cause cancer or lead to its aggressive growth in the breast. Breast tumors have been found to be correlated with imbalances in estrogen metabolism in breast tissue. Higher serum estrogen and modulation of estrogen disposition have been correlated with breast cancer development. In one study, estradiol levels were found to be two-to-ten times greater in patients with cancer than control patients. Additionally, estrogens are thought to mutate apurinic sites, initiating breast and other cancers [8]. Estrogen-related carcinogens are often indicated by

imbalanced estrogen quinones, reactive metabolites of estrogen [9]. Therefore, a sensor that tracks estrogen can serve as a biomarker for the risk of breast cancer.

In men, high levels of estradiol were correlated in patients with cirrhosis [10]. In Chopra et al., the mean serum and unbound estradiol concentrations were found to be significantly higher in men with cirrhosis than the control group. In their study, abnormal estrogen metabolism and increase in circulating estrogen were determined to be associated with the development of cirrhosis. Thus, the ratio of testosterone to estrogen in male patients with cirrhosis was much higher than the control group. The mean unbound estradiol in their male subject's serum was abnormally elevated to that of the average woman's levels during the follicular phase of menstruation. Therefore, a continuous, in vivo estradiol sensor could be used by men as a diagnostic for health issues such as cirrhosis.

Estrogen hormone imbalances can be indicative of multiple health risks. Hormone imbalances are often not detected until they severely affect the body due to their large variance of symptoms and their severity [11]. While women do experience normal hormonal imbalances during their lifetime (puberty, pregnancy, and menopause), hormonal imbalances outside of these events can be detrimental to overall health. While no one diagnostic tool can unequivocally determine a patient's condition, continuous monitoring of estrogen can provide patients and their health care providers with more information for a proper diagnosis.

1.2.3 Fertility Disorders

One of the most common fertility disorders is polycystic ovary syndrome (PCOS) [12]. According to Franks M.D., the accepted clinical definition of PCOS is hyperandrogenism associated with chronic anovulation in women without underlying adrenal or pituitary gland diseases. It is acknowledged as a hormonal disorder that causes enlarged ovaries with cysts on the distal edges. PCOS can cause anovulation, hirsutism, insulin resistance, irregular menstruation, and irregular menstruation periods. While these symptoms can be early indicators of PCOS, a full diagnosis often requires a clinical, ultrasonographic, and biochemical investigation. Symptoms of PCOS, like hirsutism and obesity, overlap with other health risks and can therefore prolong and complicate its diagnosis. Thus, PCOS will often go untreated because its symptoms can easily go unnoticed, and a full diagnosis requires multiple tests that may not be preformed unless PCOS is suspect [13].

PCOS was one of the primary inspirations for this project as it is difficult to diagnose, and no singular test serves as its diagnostic. However, PCOS could be detected with continuous monitoring of estradiol. Individuals with PCOS do not exhibit a preovulatory or midluteal increase in estradiol concentrations during their menstrual cycle [13]. Thus, continuous monitoring of estrogen levels can inform a patient and their health care provider of possible abnormal estrogen secretion that would otherwise go undetected. Currently, the only way to detect PCOS using estradiol is with multiple, well-timed blood tests.

Another chronic fertility complication is primary ovarian insufficiency (POI), also known as early menopause. It is clinically defined as the condition in which a woman

under 40 years of age expresses amenorrhea for four months or more and has two serum FSH tests result in levels in the menopausal range. When POI is suspect, initial rests are run to determine the levels of serum prolactin, FSH and thyrotropin. A clinician will take serum estradiol measurements after the FSH level is reported to be in the menopausal range; women with POI have low serum estradiol levels compared to control groups. Individuals who suffer from POI do not produce normal amounts of estrogen or release eggs, leading to infertility. Some individuals with POI have symptoms of estrogen deficiency: vasomotor symptoms, sleep disturbance, and vaginal dryness. A POI diagnosis will be confirmed if a high FSH and low estradiol level is determined. POI can be treated with estradiol hormonal therapies and supplements [14]. Therefore, an estradiol sensor could be used to measure the effectiveness of estrogen absorption during hormone therapy in addition to being used as an early diagnostic.

1.3 Current Fertility Tracking

There are various approaches to track the fertility cycle that are covered in this section. Fertility awareness methods are the most common and rely on meticulous tracking by the menstruating individual. Blood tests are not commonly used as a consistent fertility tracking solution due to its invasive nature and necessary aid from a health care professional. We also review a new solution, the Layla Wellness Intravaginal Ring which predicts fertility by measuring the viscosity of cervical mucus.

1.3.1 Fertility Awareness Methods

The calendar method, or the rhythm method, is a technique used for family planning. By tracking an individual's menstrual cycle history, ovulating individuals can predict which days they are most likely to conceive [2]. Therefore, those wishing to become pregnant can use the calendar method to target days when they should have sex, and those wishing to avoid pregnancy can use it to avoid having sex on those days. This is an at-home technique that requires accurate and steady recording of the menstrual cycle [15]. An individual can create a custom menstruation calendar based on their recorded history or use a variation of the calendar method called the standard days method. Initial tracking must be done for a few months to establish the length of the cycle which normally ranges between 26-32 days. From there, each phase of the menstrual cycle is assumed to take place within a prescribed number of days based on the first day of bleeding [16].

Users will employ the calendar method, sometimes with the aid of an app. Apps and websites available to more accurately predict fertility based on the calendar method. They are non-invasive, in-expensive, and can be used at home without a medical professional's supervision. Such tools include Clue [17], Ovia [18], and Natural Cycles [20]. Some, like Natural Cycles, include data from a basal thermometer to improve the accuracy of prediction.

Individuals can also track their fertility using the temperature method [21]. It is known that the basal body temperature fluctuates throughout the menstrual cycle, rising during ovulation [22]. Individuals wanting to become pregnant will assume that the increase in basal body temperature (approximately four-tenths of one degree) is a fertile

day and plan to conceive on those days. For the most accurate measurement, individuals are expected to take their temperature as soon as they wake-up, avoiding movement, eating, drinking, or checking the phone.

The last common method that individuals use to track fertility is the cervical mucus method [23]. The color, texture, and viscosity of cervical mucus will change throughout the menstrual cycle. Like the other fertility awareness methods, meticulous tracking is required for accurate prediction. This method often requires expertise of a health care professional to accurately determine the characteristics of the cervical mucus and its relationship to the menstrual cycle.

In general, fertility awareness methods are only 76-88% effective [2]. These methods are imprecise because they do not measure the hormone levels in the body which are the determinants of fertility.

1.3.2 Blood Tests

Unless a health risk is assumed, blood tests for the purpose of fertility tracking are less common than fertility awareness methods [24]. However, bloods tests are the most accurate predictor of an individual's fertility status because they directly measure hormones. Luteinizing Hormone (LH) and Progesterone levels will be tracked through blood tests to determine the body's ability to release an egg and sustain it in the uterus, respectively.

The term blood test incorporates multiple measurement techniques for detecting estradiol in serum: bioassay, mass spectrometry, UV absorbance, immunoassay, and radioimmunoassay. Today, blood tests are mostly direct assays, meaning that the

estradiol does not need to be isolated from the serum itself. These types of tests are mostly enzyme-based immunoassays. However, mass spectrometry is becoming more widely used, even though it requires an extraction and chromatography pretreatment, because it has high specificity and sensitivity [25].

Estradiol blood tests are used to assess health risks in men and women. In the context of fertility tracking, they are used to measure effectiveness of hormone therapy or fertility treatments: E2 levels will be monitored over the course of multiple blood draws to establish ovarian function. Due to the expense and invasive nature of blood tests, individuals will likely not use continuous blood draws as a fertility tracker despite its accuracy.

1.3.3 Layla Wellness Intravaginal Ring

PreOv is currently in development, made to aid with fertility tracking [26]. PreOv's foundation is in the cervical mucus method. The device aims to provide objective information about the consistency of cervical mucus. PreOv is an intravaginal ring that monitors the viscosity of cervical mucus through impedance. The impedance of cervical mucus changes with the volume and ionic content due to changes in sodium chloride and the estrogen: progesterone ratio [27]. PreOv eliminates the subjective interpretation of cervical mucus by basing its predictions solely on impedance throughout the cycle. The device is to be implanted for a two-week period and provide continuous impedance, and prediction information, to a phone application.

1.4 Conclusion

This thesis will hopefully serve as the inception of in vivo estradiol monitoring. Estradiol is a sex hormone that is present in all individuals, influencing the menstrual cycle and overall health. Therefore, it is of interest to develop a continuous monitor for estradiol which can serve as a diagnostic tool for various health risks or family planning. It is the goal of this thesis to determine the feasibility of an electrochemical estradiol sensor with the intention of being integrated with an implantable device, such as PreOv.

CHAPTER 2

APPLICATION REQUIREMENTS

2.1 Introduction

This chapter provides background information regarding the various components of an electrochemical sensor and its needs for fruition. First, we explicate the nature of estradiol and its relation to the menstrual cycle. Then, we define the physical requirements that the sensor must fulfill for implantability: size, shape, access to biological fluid, power, and the ability to equilibrate.

2.2 Estradiol in Context of Sensor Specifications

Estradiol, $C_{18}H_{24}O_2$, is the female sex hormone primarily responsible for the menstrual cycle. It is also referred to as beta-Estradiol, 17β-Estradiol, oestradiol, and E2 [1]. Estradiol is produced by the ovaries to bind to and activate particular nuclear receptors that cause the maturation and release of an egg [28]. Compared to other commonly measured molecules, estradiol is a relatively small particle, with a molar weight of 272.4g/mol, and a topological polar surface area of 40.5 $Å^2$. Estradiol is one of three estrogen types: estradiol, estrone, and estriol. While each estrogen has similar structures and functions, estradiol is the most potent in non-pregnant women and significant in determining fertility which is why it is the focus of this thesis [29].

Estradiol, along with the other female sex hormones (luteinizing hormone, follicle-stimulating hormone, progesterone) fluctuates throughout the menstrual cycle [30]. Therefore, an effective sensor shall detect fluctuations by differentiating between the various levels of estradiol. The menstrual cycle usually takes place over the course of 28 days and is composed of two subphases: follicular and luteal. The follicular phase is the phase in which estrogen increases in preparation for the release of the egg. It includes the period and the proliferative phase, the shedding and rebuilding of the uterine lining. The luteal phase has an increase in progesterone, preparing the body for pregnancy. It includes the secretory phase in which the uterine lining secretes chemicals that will support pregnancy in the event of implantation or will prepare the lining to be broken down. The luteal and follicular are separated by the ovulation event which is triggered by a spike in luteinizing hormone [31]. The time in which an individual is most fertile, and likely to become pregnant, is during the ovulation window [32]. Table 2.1 summarizes the time of each of these phases [33].

The amount of time spent in each phase will vary from individual to individual [33]. Knowing the length of these phases, and assuming that ovulation occurs on the day of the LH peak, we can map estradiol, and other hormones, to the known menstrual cycle (see Figure 2.1).

Table 2.1 Time of each phase of the menstrual cycle

Phase	Days
Total Cycle	25-30
Follicular Phase	10-16
Luteal Phase	~14

LH, FSH, estrogen, and progesterone rise and fall throughout the menstrual cycle, inducing the release of the egg, the growth of the uterine lining and the disposal of both upon lack of fertilization. Estradiol's maximum is during ovulation, and minimum is during the transition between the luteal and follicular phase, day 24 to day 8 according to Figure 2.1. In a study performed by Stricker et.al, the maximum mean estradiol over the menstrual cycle was 914.84pmol/L, occurring during ovulation; the minimum mean estradiol over the menstrual cycle recorded was 118.42 pmol/L occurring on the first day of the follicular phase. The Stricker study included 20 participants, however, the averaged minimum value only included 8 participants. Excluding days where less than 19 participants were used, the minimum recorded estradiol level was 49.91 pmol/L, and the maximum recorded estradiol level was 1884.91 pmol/L from the Stricker study [30].

Estradiol also fluctuates on a diurnal cycle. According to a clinical study by Bao et al. [35], the peak of estradiol was found to occur between 6:00AM and 9:00AM, at approximately 55.07pmol/L. After this peak, 3-hour period oscillations occurred for the rest of the day with an average of 14.68pmol/L. Only 15 of the 53 subjects participated in

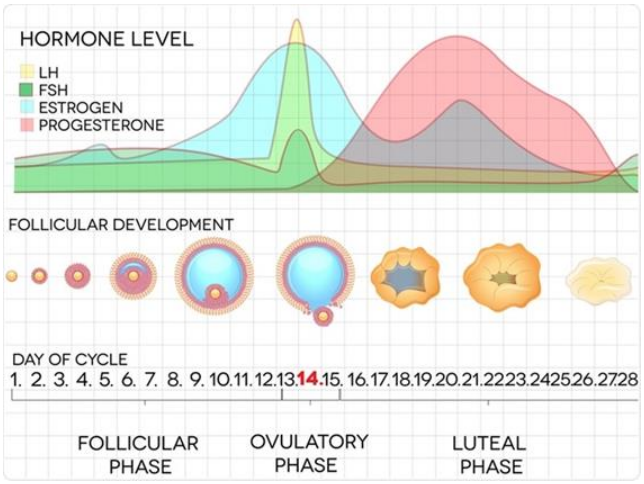

Figure 2.1: Hormone levels throughout the menstrual cycle [34]

the study during their suspected ovulation period, possibly skewing the data, and explaining why the values are lower than the mean estradiol minimum for the Stricker study. Regardless, it is important to note from this study that the estradiol levels in an individual can greatly vary throughout the day and it is imperative that an estradiol sensor have the capability to detect the changes occurring throughout the day. Without this capability, the estradiol level recorded for a particular day cannot be properly contextualized in the entire cycle. Essentially, if a user or health care provider cannot take a measurement at the same time each day or have multiple measurements to account for the diurnal fluctuations, a singular measurement may be convoluted and inaccurate as a daily total.

From these studies, we can determine that an accurate estradiol sensor must be able to take multiple measurements throughout the day with a limit of detection of 10pmol/L in order to meet the oscillation limit of 14.68pmol/L from the Bao study, with room for error. We hypothesize that detection range of 10pmol/L to 1000pmol/L will capture at least 95% of the data.

We consulted a clinician and asked what sampling rates would be acceptable from a user and health care provider perspective. The minimum ideal sampling rates dependent on use from Jeanna Tachiki Ryan, an adjunct instructor at the University of Utah and Physician's Assistant, are summarized in Table 2.2 [36].

In general, Tachiki Ryan emphasized that from a healthcare provider's perspective, it is most important to be able to control when the sample is being taken for diagnosis. This allows the healthcare provider to target a particular time/day of the cycle for their evaluations. The diurnal study performed by Bao et al. took samples at two-hour

Table 2.2: Expert recommendation for sampling rate on estradiol sensor

Use-Case	Ideal Sampling Rate
General clinical evaluation	6 hours
Fertility treatments: IUI, IVF, ovarian simulation	6 hours
Fertility tracking	6.5 hours
Menopause diagnosis	24 hours
Labor prediction	24 hours

intervals because they determined that there was no significant change to the concentration of estradiol smaller than that time step. Therefore, for the sensor to provide the largest amount of unique data points, it would ideally take a sample every two hours. To still be considered a useful continuous-sampling sensor for users and clinicians, the minimum sampling rate would be 24 hours; however, the applications become more limited as the sampling interval increases.

The feasibility of a 2 to 24 hour sampling rate is dependent on the sensor's time delay. The association and dissociation rate constants of the aptamer dictate how accurate the capacitance reading is in regards to the actual level of estradiol present in the body. We want to sample at a frequency that optimizes accuracy and is useful for clinical application.

2.3 In Vivo Needs

For the sensor to work in vivo, it must be implantable and have access to biological fluid. In blood, estradiol is commonly bound to sex hormone binding globulin and albumin [37]. Currently, only estradiol that is unbound or bound to sex hormone binding globulin is bioavailable for sensing [38]. It is our goal to sense the free estradiol as it is the only type that is accountable for endocrine regulation [39]. However, only

1.5% of total estradiol in the blood is unbound [40]. Therefore, if the sensor is only able to access 1.5% of estradiol in the system, then it must have a limit of detection low enough to account for a low concentration. Otherwise, it must be able to sense bound estradiol, or be able to break the bonds of bound estradiol. At the time of this thesis, we were unable to find a study reporting the bioavailability of estradiol in cervical mucus; thus, it assumed that the percentage of unbound estradiol in cervical mucus is approximately that in serum, 1.5%.

As an ex vivo alterative, the sensor could use saliva as its biological fluid. At sufficiently high concentrations (~1800pmol/L), serum estradiol correlates well with salivary estradiol (R^2=0.74) [37]. Therefore, if food intake is controlled for, saliva can be a good surrogate for serum when sensing free estradiol.

For a sensor to have access to serum or cervical mucus it must satisfy a size restraint to be implantable. Nexplanon, a birth control that is inserted into the upper arm, is 4cm in length and 2mm in diameter [41]. The Eversense CGM is a diabetes glucose sensor that is inserted in the same location, measuring 18.3mm in length and 3.5 mm in diameter [42]. The Nexplanon and Eversense are shown in Figure 2.2.

These sensors have a similar, simple insertion procedure: a small incision perpendicular to the arm is made, then the applicator is inserted into the incision and pushes the sensor into position into the subcutaneous tissue [44]. However, the Eversense glucose monitor is only inserted for 90 days, while the Nexplanon can last for up to four years. Therefore, to have symmetry among other commercially available arm implants, we would want our sensor to be cylindrical for easy insertion with preexisting applicator designs, and under 400mm in length and 4mm in diameter. If the device were to be a

Figure 2.2: Nexplanon (left): cylindrical upper arm birth control implant [41]. Eversense CGM sensor (right): cylindrical upper arm diabetes monitor implant [43].

cervical implant, its shape would vary but its scale would be the same. Common cervical implants are intrauterine devices (IUD) which vary from 28-32mm by 30-36mm [45]. IUDs have two arms, forming a T-shape (see Figure 2.3).

During insertion if an IUD, a speculum is used to hold the vagina open as the applicator is inserted past the cervix and releases the IUD into the uterus [47,48]. The Nuvaring, an intravaginal ring that is used as hormonal birth control, has an outer diameter of 54mm and a cross-sectional diameter of 4mm [49].

The intravaginal ring being developed by Layla Wellness has an outer diameter of 55mm, and a cross-sectional diameter that varies from 4mm to 12mm [36]. An image of the Nuvaring and a schematic of the Pre-Ov ring are shown in Figure 2.4. Intrauterine and

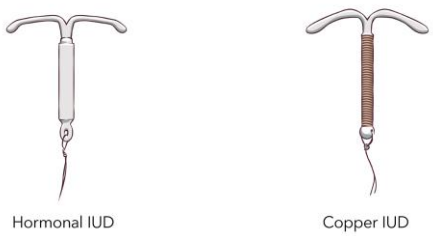

Figure 2.3: T-shaped IUDs [46]

intravaginal options are convenient because they do not require incision and can accommodate slightly larger device sizes.

The detection method in this thesis is through cyclic voltammetry, an electrochemical test performed by a potentiostat. The plots produced from these experiments are called cyclic voltammograms (CVs). At the time of this thesis, the smallest commercially available wireless potentiostat is the ECWP100S Connector made by Zensor; it is 61x20x19.5mm [51]. Assuming that the ECWP100S Connector could be modified for implantation, the estradiol sensor would at minimum be approximately the same size.

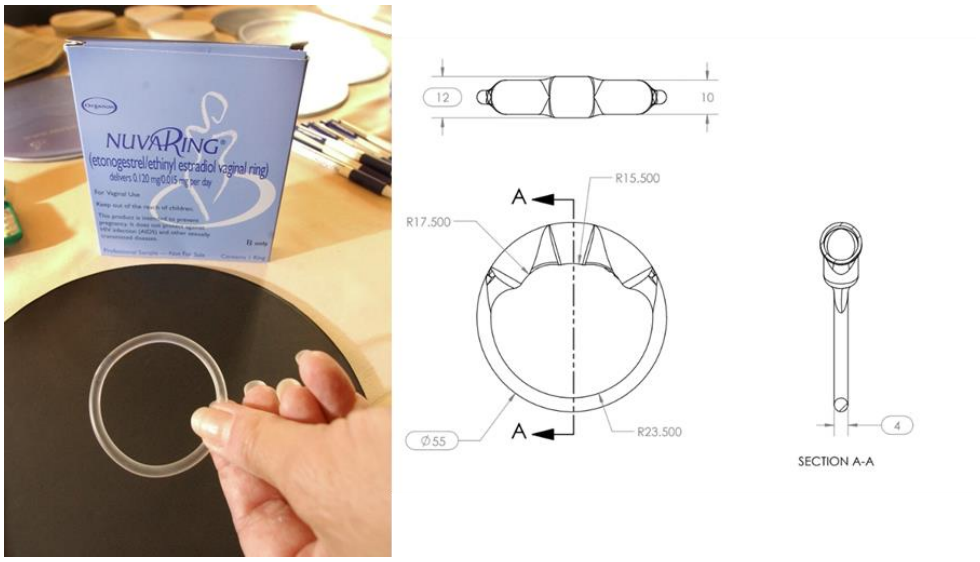

Figure 2.4: Nuvaring [50] (left) and Pre-Ov ring [36] (right) both have a circular shape that can easily conform to the vaginal canal

2.4 Power Requirements

The power required for this sensor is necessary for cyclic voltammetry and information transmission. The Connector of the ECWP100S is a self-contained potentiostat and transmitter requiring DC 5V and 0.5A. This provides battery life between 1-6 hours. If the estradiol sensor was able to be recharged while in vivo using wireless power transfer, the battery used for the ECWP100S Connector would likely be sufficient. The Eversense glucose sensor is powered by its external transmitter with rechargeable lithium polymer batteries which are then charged by a power supply using AC Input, 100-240Vac, 50/60Hx, 0.3-0.15A. Under a single charge, the sensor and transmitter can function for up to 42 hours. It is unclear what the exact battery used for the Eversense sensor is, but we know that it requires power in the milliwatt range, similar to implantable drug delivery systems which commonly use Lithium/Manganese dioxide batteries [52].

2.5 Equilibrium and Other Specifications

Our goal is to develop a sensor that requires no reset or intervention to run multiple measurements; we define this as an equilibrium sensor. Under our definition, an equilibrium sensor is able to establish a baseline, and fluctuate according to the body's estradiol concentration (equilibrate), without intervention. For our sensor, this is a cyclical process of association, and dissociation achieved by aptamers; our sensing mechanism is detailed in Chapter 3.

Equilibrating without intervention is crucial for our goal of in vivo continuous sampling. An implantable sensor is unable to be cleaned or replenished in between

samples. Thus, the sensor must be able to associate, and disassociate with biologically safe procedures and materials capable by the sensor from implantation. An implantable sensor designed to take samples every two hours for the entirety of a menstrual cycle (~30 days) must be able to take a sample 360 times.

If the sensor were to be adapted into a gated microfluidic chip, then the aptamers would have to be able to be exposed to biofluid approximately 360 times. In this scenario, a valve would open to allow a small sample of biological fluid to enter the chip to be tested, then a second valve would open after the CV is taken so the sample could be pumped out. This type of sensor adds complexity to the design of an implantable but would reduce the number of associations and dissociations to a value that a field of aptamers may be more likely to achieve on average. Conversely, if the sensor did not possess any filtration mechanism then the aptamers would be exposed to biological fluid constantly, and require many more association and dissociation events over their lifetime. Despite the sensor only sampling approximately 360 times over its lifetime, the aptamers' constant exposure to biological fluid allows the aptamers to always be available to be bound and then released.

By making an equilibrium sensor, we achieve continuous monitoring for extended periods of time without removal from the body. Less disposable materials cut down the monetary cost, and less insertion/removal procedures cut down physical cost. The equilibrium sensor provides a less invasive solution for users that want to be able to track their estradiol levels from home without requesting such information from their clinician.

The ability for the sensor to equilibrate is dependent on the association and dissociation rates, explored in Chapter 4. We assume that we will be able to take a sample

every two hours and satisfy the clinical time requirements. If the sensor is unable to associate and disassociate naturally within a reasonable amount of time, the reported estradiol concentration will be inaccurate. In such a case, we hypothesize that delivering a small electric shock to the system can induce a dissociation event. The aptamers fold when bound to estradiol, bringing their negatively charged backbone towards the electrode surface. Hypothetically, an electric shock from the electrode surface could push this negatively charged backbone away from the electrode surface, causing the aptamer to unfold and break its bonds with the estradiol molecule.

Additionally, the sensor's dissociation capabilities dictate the sensor's lifetime and the complexity of the chip's design. We did not determine if the aptamers denature after a particular number of association/dissociation events, or due to amount of time spent in the electrolyte. Further experimentation would need to be performed to determine how many samples the sensor can take continuously. We cannot conclude from our current study that the aptamers are able to associate and disassociate more than once. An experiment to determine the average number of exposure events capable by the sensor would consist of: the sensor is exposed to an estradiol concentration for ten minutes, then allowed to dissociate for two hours, and then exposed to a new estradiol level for ten minutes. This would be repeated for an extended period of time while measurements are taken after each concentration change. If it is determined that the aptamer field cannot withstand enough exposure events to stay accurate throughout its lifetime, then a shorter implantation lifespan, new sensing mechanism, or ex vivo alternative must be explored.

The sensor's lifetime is also dictated by the amount of power we can supply, susceptibility to biofouling, strength of the thiol bonds (see Section 3.2.4), in addition to denaturing.

Ideally, the sensor would be able to differentiate the smallest step in concentration between two samples during the diurnal pattern, 3.5pmol/L [34]. During the Bao et al. study, a two-hour sampling interval was determined to be the most frequent sampling interval that provided unique information about the status of estradiol in the individual. The smallest step in concentration observed during the study was 3.5pmol/L. Therefore, a difference of 3.5pmol/L provides unique information about the levels of estradiol in an individual and should be captured by the sensor; the resolution of the sensor ideally should be 3.5pmol/L. In a 24-hour period, a difference of 3.5pmol/L is meaningful. However, from a monthly perspective, the phases of the menstrual cycle change on the order of hundreds of pmol/L. Therefore, a resolution of 100pmol/L would be needed if we were only interested in differentiating between the phases of the menstrual cycle. Ideally, however, the sensor would be able to track the daily fluctuations to provide context to the monthly fluctuation and thus needs a smaller resolution.

The sensor should also have a high specificity and stability, and a relatively low signal to noise ratio (SNR). Aptamers are often chosen as the sensing mechanism for biosensors due to their innate specificity. The high specificity of an aptasensor is due to the process in which the aptamer is defined through systematic evolution of ligands by exponential enrichment (SELEX); its fabrication requires multiple iterations to find a nucleotide specific sequence specific to the target molecule [53]. Specificity should be maximized; conversely, drift and noise should be minimized. Under these assumptions,

for our sensor to be considered stable, the drift must be smaller than the smallest step size, 3.5 pmol/L. For our purposes, the SNR can be evaluated through a qualitative evaluation of the individual CVs. The CVs are examined for noise under two criteria: width of band, and variation between two points directly next to one another. A thick band with highly variable adjacent capacitance values will produce a fuzzy appearance. If this fuzzy appearance is recognized, the CV will be discarded from the overall dataset.

2.6 Conclusion

The sensor ideated in this study must satisfy multiple design constraints in order to be specific to estradiol, useful to a clinician, and implantable. To be used as a fertility tracker or diagnostic tool, the sensor must be able to sense estradiol at its various levels throughout the menstrual cycle. For the ideal use case, the sensor would be implanted for the entirety of a menstrual cycle and able to take a measurement every two hours. The shape of the sensor is dependent on the location of implantation but would have to be on the order of mm. Additionally, the sensor's power requirements must be minimal to accommodate implantability. The application requirements according to an implantable estradiol sensor's needs, are summarized in Table 2.3.

Table 2.3: Summary of theoretical application requirements

Need	Requirement	Property
Can sense the small molecule of estradiol	A sensing mechanism must be specific and selective to estradiol	Aptamers
Complete tracking of menstrual cycle	Sensor's lifetime must capture the luteal, follicular and ovulation phase	Sensor implanted for thirty days
Can differentiate between different phases of menstrual cycle	Sensor must measure multiple discrete levels of estradiol	Sensor's limit of detection should be 10pmol/L with a range of 10pmol/L to 1000pmol/L
Relevant information for clinicians	Sensor must take a measurement frequent enough to be useful to a clinician	Sensor takes a measurement at least once every twenty-four hours
Access to biological fluid	Sensor must be implanted in a location where biological fluid is easily accessible	Implantation site of sensor is either the upper arm or inside the vaginal canal
Physically implantable	Sensor must be small enough to be easily implanted and shaped ergonomically	The length and diameter should be on the order of mm. Depending on implantation site, the shape should be a cylinder or ring.
Power for cyclic voltammetry and information transmission	Sensor must have a battery that can either be recharged or last for the duration of its lifetime	The sensor's power should be low enough to be able to operate for the entire lifetime of the sensor
Reusability	Sensor must continuously sample without replenishing materials which would require the implant's removal	Aptamers must be able to associate and disassociate many times

CHAPTER 3

SENSING MECHANISM

3.1 Literature

The inspiration for the sensing mechanism on this project came from the three papers detailed in the following sections. Procedures, methods, and materials from the literature were adapted into this study to create a three-electrode electrochemical sensor that utilizes aptamers and cyclic voltammetry.

3.1.1 MEDIC

The *Real-time, aptamer-based tracking of circulating therapeutic agents in living animals* by Ferguson et al. 2013 introduced us to the idea of using aptamers as a sensing mechanism [54]. This study covers the development of a microfluidic electrochemical sensor for in vivo continuous monitoring of drugs in whole blood. The novelty of the sensor is that it can work in-vivo, in real-time, and has the potential to sense many types of biological molecules. The original intent of this thesis was to modify the microfluidic chip Ferguson el. al developed to be compatible for sensing estradiol.

Their microfluidic chip is referred to as the MEDIC device and is composed of a three-electrode system patterned onto borofloat glass wafers using photolithography and electron beam evaporation. The chip has a series of channels that serve as a continuous

flow diffusion filter to prevent other biological material from coming in contact with the working electrode surface. The MEDIC has an Ag/AgCl reference electrode, a platinum counter electrode, and a gold working electrode on which the aptamers are immobilized. The team designed MEDIC to allow the working electrode to be interchangeable so different aptamers could be used, thus different molecules could be sensed. While this paper does not use estradiol, the method of using three-electrode voltammetry as an aptasensor was adapted into this study's methods.

3.1.2 CNT FET

A carbon nanotube field effective transistor (CNT FET) was used as an aptasensor in the study *Back-gated Carbon nanotube field effect transistor aptasensors for estrogen detection in liquids* by Zheng et al. [55]. This study was motivated by the need to detect hormones in waterways, which has been proven to have adverse effects on health. Zheng et al. functionalized a 100x10µm area of a CNT FET with aptamers specific to estradiol. This paper corroborated that an estradiol aptamer would behave similarly to the aptamers used in the MEDIC study: a physical conformation change would induce a change in current.

This device used a 35-mer aptamer sequence to detect estradiol at a concentration between 50nM and 1.6µM. The aptamers are functionalized on to the CNT surface. When the negatively charged aptamers bind to estradiol, a folding confirmation change brings the negatively charged aptamer closer to the CNT surface. This conformation change alters the charge distribution in the electric double layer (EDL). The thickness of the EDL is the Debye length. If binding events take place within the Debye length, a

change in current response will be observed for the CNT FET due to the effective change in the gate potential. Similar to the MEDIC device, the current and potential increase with the concentration of the particles of interest due to the folding of the aptamer. Our study aimed to incorporate the real-time detection capabilities of the CNT FET device with biocompatibility by avoiding using CNT.

3.1.3 EIS

The last paper that inspired our study's methods was written by Li et al. in 2016, *Sensing Estrogen with Electrochemical Impedance Spectroscopy* [56]. Similar to the CNT FET study, this study was concerned with detecting estradiol as a pollutant; however, the Li study detected estradiol in gaseous phase. The limit of detection from this study, $3.7x10^{-4}$ng/L (1.4pmol/L), is relatively low because Electrochemical Impedance Spectroscopy (EIS) was used as the sensing mechanism. We were interested in this paper's methods due to its sensing mechanism's relatively low limit of detection.

ElS was conducted using a three-electrode system consisting of an Ag/AgCl reference electrode, a platinum counter and gold working electrode on which estrogen receptor-α (ER- α) was immobilized. ER- α is a nuclear receptor specific for estradiol. Nuclear receptors are proteins; thus, they differ from aptamers which are comprised of nucleotides. When estradiol binds to the proteins' receptors, it hinders diffusion of $[Fe(CN)_6]^{3-}/[Fe(CN)_6]^{4}$, thus increasing the impedance of the system. As the concentration of estradiol increases, more receptors are bound, and the diameter of the Nyquist plots linearly increase. This sensor is inverse to the CNT FET and MEDIC sensors because the sensing mechanism prevents the flow of electrons instead of aiding

the flow of electrons.

We explored EIS as a system for detection, but moved away from it as it proved to be less consistent than cyclic voltammetry.

3.2 Experiments

The following subsections define the materials and procedures used in this thesis. The last subsection provides the results and explanation of the results from the detection experiments.

3.2.1 Define Aptamer

Aptamers are specific single-stranded nucleic chains used to detect various biological molecules. They are commonly used for the detection of pathogens (E. Coli, mycobacterium tuberculosis etc.) and viruses (herpes, hepatitis B&C, HIV, SARS coronavirus) due to their versatility for detecting many different molecules, small size, and compatibility for thiol-immobilization [57]. Additionally, they have high specificity and selectivity, making them a reliable sensing mechanism.

Aptamers are determined through SELEX. SELEX was performed by Eisold et al. to determine a 35-base nucleotide sequence for the estradiol aptamer used in this study, shown below [58]:

5-AAGGGATGCCGTTTGGGCCCAAGTTCGGCATAGTG-3

This configuration allows both the 5’- and 3’- end to be used for immobilization. The sequence used in our study is slightly modified to include a fluorescent marker (FAM) on the 5’ terminal and a C6-S-S group on the 3’ terminal to aid with thiol

bonding. Therefore, our aptamer is immobilized to the electrode surface on the 3’- end. Our aptamer was produced by the University of Utah’s Health and Science Center DNA Sequencing Core Facility. Small terminal groups have been found to have little to no effect on packing density [57]. There are five unbound bases at the ’'-end and four unbound bases at the 3’-end. This, along with the stem region with six intramolecular base pairs, asymmetric interior loop and step-loop, allow the aptamer to have its unique folding characteristics specific to estradiol. The binding site for the estradiol is at the asymmetric interior loop and the step region. The bases specifically interacting with estradiol are: G22, T12, T24, and C26. Table 3.1 summarizes the types of bonds formed between the bases and estradiol.

In Eisold et al., coarse-grained modelling methods determined the estradiol aptamer’s final structure: RNABuilder was used to predict and model the base pairs of the DNA structure and PLIP was used for interactional analysis between the aptamer and E2. Using these modelling tools, the simulation determined that estradiol would bind to the aptamer in over 99% of cases. Additionally, the simulation determined that 98.12% of all H-bonds were formed by T12 and C26, and 89.27% of all pi-stacking interactions were formed by T24 [58]. In vivo, fouling in the form of nonspecific binding can occur due to other proteins like albumin, globin, cholesterol, LCL, HCL etc. found in human serum [57].

The capacitance value from aptamer response is a spatially averaged response from the aptamer field on the surface of the electrode. It is important to know how the field will respond given a concentration. The fraction of bound aptamers can be mapped to the corresponding capacitance value and target (estradiol) concentration.

Table 3.1: Bonds formed between aptamer and estradiol molecule at corresponding bases

Bases	Bonds
G22	Hydrophobic interactions, water-mediated H-bonds
T12	Hydrophobic interactions, water-mediated H-bonds, H-bonds
T24	Pi-stacking interactions
C26	H-bonds
other	Non-covalent bonds

The physical confirmation change will increase the capacitance of the system, and thus increases the amount of current able to flow into the system. The aptamer folding makes the aptamer monolayer thinner, decreasing the distance between the electrode and ions in the electrolyte. Therefore, a higher concentration of estradiol means more molecules of estradiol which will cause more aptamers to fold and more current to flow. Thus, an increase in capacitance is directly proportional to an increase in the concentration of estradiol.

In order for the capacitance change to be detected by the three-electrode system, the aptamer must first be immobilized onto the working electrode's surface; this procedure is detailed in Section 3.2.4. In this procedure, the self-assembled monolayer (SAM) of aptamer is backfilled with mercaptohexanol (MCH). An SAM is generally created by the adsorption of sulfur molecules onto an inert metal surface. Herne and Tarlov [60] introduced this backfilling method to displace nonspecifically adsorbed aptamers. Backfilling spaces the aptamers to ensure an upright orientation and provides room for the aptamers to fold. Thiolated aptamers will nonspecifically adsorb to the surface through their Nitrogen atoms; backfilling prevents this nonspecific adsorption from restricting the accessibility of the analyte to the aptamer [58]. The density of the

working electrode surface must be balanced: it should be as dense as possible to provide high sensitivity, but as sparse as possible to prevent steric hindrance [61].

The stability of the SAM comes from the strong covalent bonds created between the gold and thiol, an Au-S bond [62]. In this study, the SAM is formed in three steps: physio-absorption, chemisorption, and a crystallization process. The physio-absorption is diffusion-controlled, and only uses Van der Walls interactions. The chemisorption step is when a mercaptan-hydrogen atom loses its sulfur head and then bonds to three gold atoms. Lastly, the crystallization process uses Van der Walls, repellent, steric, and electrostatic forces to align the surface molecules in a parallel tail-tail monomolecular layer.

Various SAM defects such as disordered rows, pinholes, and rows of missing molecules can foul the system. Diao et al. determined that by extending adsorption time to an hour or more, the monolayer becomes free from measurable pinholes [63]. In their study with an ODT solution, fractional coverage, pinhole size and separation were measured as a function of time in the submersion of an ODT solution. They determined that the monolayer is formed in two steps: initial and secondary adsorption. The initial adsorption occurs very quickly and accounts for most of the monolayer's coverage but is loosely packed. The secondary adsorption remedies these impurities. Thus, our study uses a 14-hour window for the aptamer monolayer to be adsorbed followed by an hour exposure of MCH to backfill and limit the possible impurities on the electrode surface.

3.2.2 Define Cyclic Voltammetry

Cyclic voltammetry is an electrochemical process that measures the resulting current when cycling the potential of an electrode system. For this study, a three-electrode system is used; thus, the following description of cyclic voltammetry will be specific to that configuration. Cyclic voltammetry is conducted using a potentiostat. The equivalent circuit is shown in Figure 3.1, below. The general equivalent circuit for a three-electrode system is shown in Figure 3.2. Table 3.2 lists the symbols and their meanings for these two figures.

The three-electrode system used in this study consists of a gold working electrode, an Ag/AgCl reference electrode and a platinum counter electrode. The aptamers coat the gold working electrode's surface. Current enters the system through the working electrode; it serves as the surface for the redox reaction. We chose a gold electrode because it is redox inert and thiol bonding, necessities for the aptamer immobilization process. The reference electrode allows the current to pass across it, but no current passes through it. The reference electrode has a low impedance to create a defined and stable equivalent potential that the working electrode can be measured against. The counter electrode completes the circuit—it is the surface to which the potential is applied as a function of the reference electrode potential.

From Figure 3.2, C-WE and C-CE represent the double-layer capacitance of the working and counter electrode, respectively. The double layer is formed due to the electrons on the electrode and the ions in the electrolyte. The molecules that attach to the surface of the electrodes act like the dielectric of a capacitor. R-WE, R-CE, and R-RE represent the charge-transfer resistance of the working electrode, counter electrode, and

Table 3.2: Symbols and Definitions for Figure 3.1 and 3.2

Symbols	Definitions
WE	Working electrode
CE	Counter electrode
RE	Reference electrode
S	Solution
C	Capacitance
R	Resistance
I_F	Current
V_{cell}	Desired cell potential

reference electrode respectively. This is the resistance of electrons shifting between the electrodes and the electrolyte. R-S represents the resistance of the solution.

The Nernst equation (Equation 3.1) describes the redox reaction that drives cyclic voltammetry: Where E is the overall potential, E^0 is the potential under standard conditions, R is the universal gas constant, T is the temperature, n is the number of electrons transferred in the reaction, and F is the Faraday constant.

$$E = E^0 + 2.3026\left(\frac{RT}{nF}\right)\log_{10}\left(\frac{Fe^+}{Fe}\right) \quad (3.1)$$

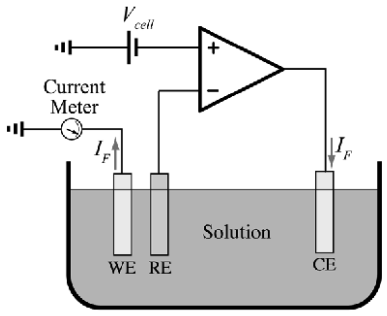

Figure 3.1: Conceptual diagram of potentiostat and three-electrode system [64]

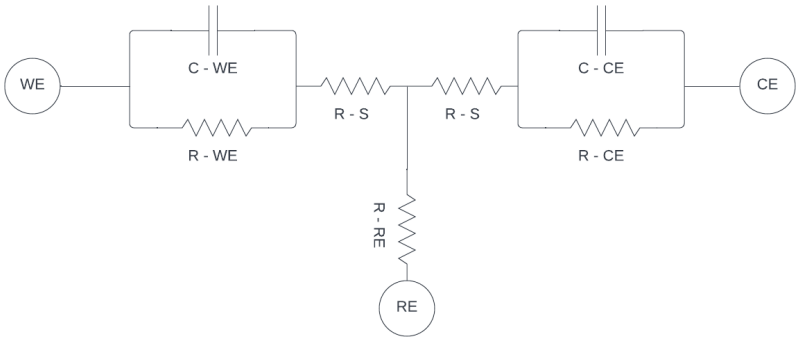

Figure 3.2: General equivalent circuit for three-electrode system [64]

The Nernst equation describes the change in concentration of Fe^{+} in a solution. Both Fe and Fe^{+} are relative to the applied potential, species, and distance between the electrode surfaces. The redox reaction is the process of potential being applied until the concentration of Fe^{+} reduces to equal that of Fe. Essentially, the energy of electrons and their resulting transfer is controlled by increasing and decreasing the applied potential until redox occurs.

A good voltammogram is evenly balanced on both sides of the x-axis. Using the US standard, the reduction portion of the trace is recorded above the x-axis and the oxidation is recorded below the x-axis. An example of a good, evenly balanced voltammogram from our experiments is shown in Figure 3.3.

Like other types of signals, a voltammogram can be influenced by noise and yield a poor trace. By cleaning the leads from the potentiostat and ensuring a rigid connection, external noise can be limited. An example of an unusable voltammogram due to noise is shown in Figure 3.4. The bands of the CV from Figure 3.4 are much thicker and fuzzier than the other traces, for our analysis it is unacceptably noisy.

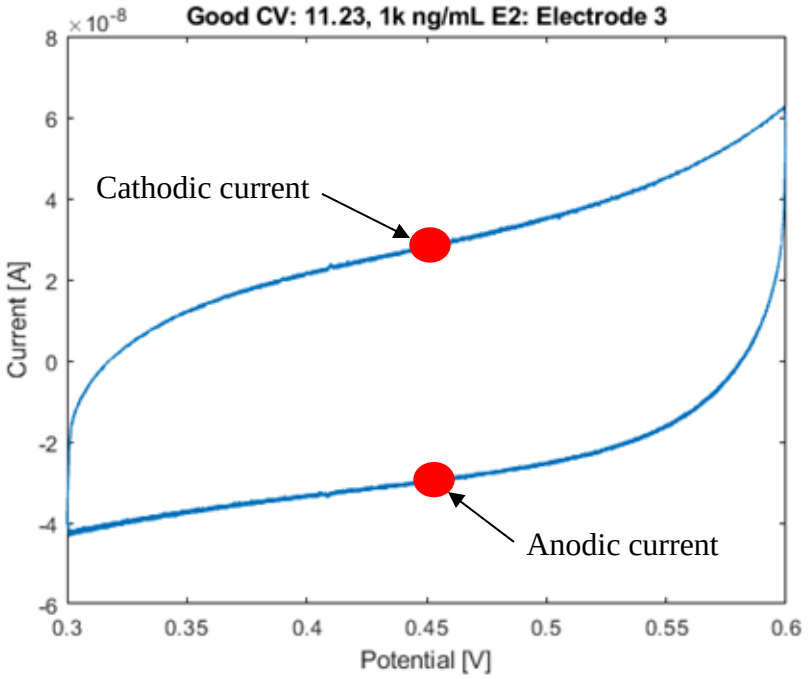

Figure 3.3: Example of a trial with a good CV—not noisy, shaped well, and balanced over the x-axis with annotations of cathodic and anodic current.

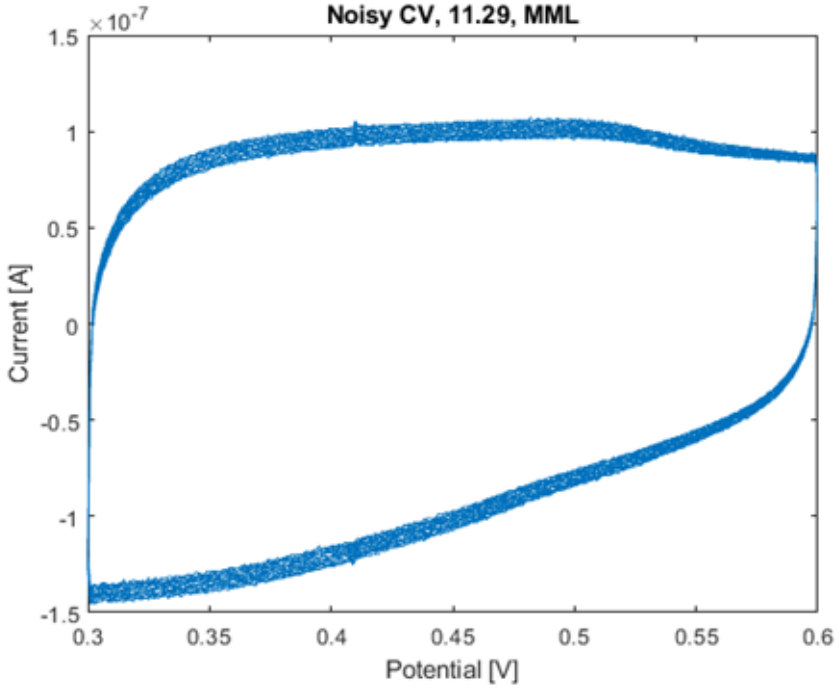

Figure 3.4: Example of a trial discarded due to noise. This particular trial is from 11.29.21, electrode 2, testing the mixed monolayer electrode condition.

Because cyclic voltammetry is an iterative process, the individual traces should overlap. There will always be some variation between cycles due to the growth of the diffusion layer. To ensure that we are recording the system's true capacitance, we only use the last 9,750 segments out of 29,750 total segments so the system has time to reach steady-state.

The shape of the three-electrode system's CV should closely mirror the CV of a capacitor (i.e., a rectangle). The equivalent circuit includes resistors, which cause a slight incline to the rectangular shape. Transient factors or a high R-S and R-RE and a low R-WE and R-CE resistor value could cause the CV to take on an irregular banana-like shape. An irregularly shaped trace should be discarded. An example of an unusable trace due to irregular shape is shown below in Figure 3.5.

We are using the capacitance of the working electrode surface as our sensing

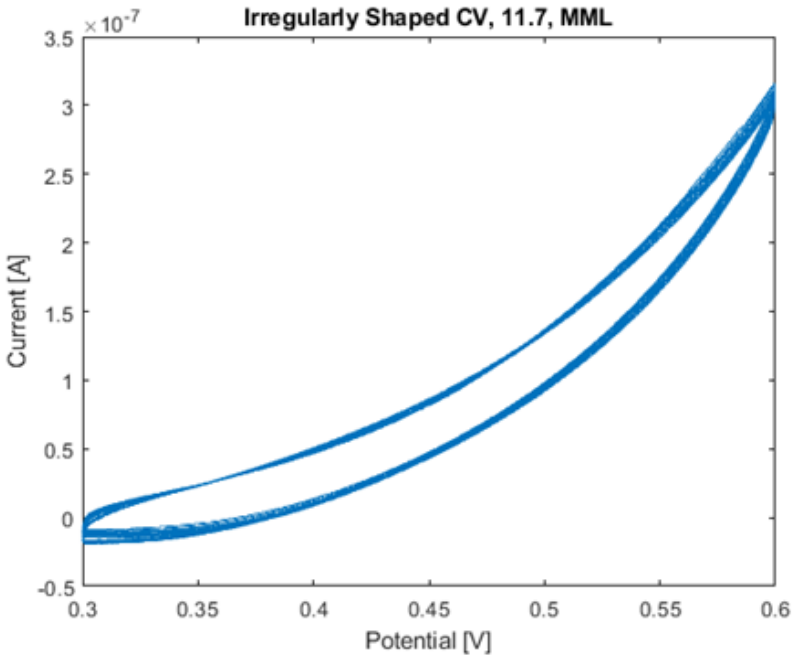

Figure 3.5: Example of a trial that should be discarded due to its irregular shape.

This trial is from 11.7.21, electrode 3, testing the mixed monolayer electrode condition.

criterion. We expect the reported capacitances to indicate discrete difference between the electrode conditions. The capacitance is calculated using the difference between the cathodic (top line of CV) and anodic (bottom line of CV) current. *I* is the difference between the two red markers from Figure 3.3. Equation 3.2 is rearranged to find the parameters of interest along with Equation 3.3:

$$I = C(\frac{dE}{dt}) \tag{3.2}$$

Rearranged:

$$C = \frac{I}{\frac{dE}{dt}}$$

$$B = \frac{C}{A} \tag{3.3}$$

When referring to capacitance in this thesis, we are referencing the capacitive density in units of μF/cm^2, B. This allows us to report the capacitance, C, in context of the surface area of the working electrode, A. Table 3.3 lists the variables, their physical meaning, and the predetermined values for Equations 3.2 and 3.3.

The capacitance and current are unique to each trial and thus do not have a predetermined value. The scan rate, 50mV/s is held constant throughout each trial, chosen to match the value from previous studies using cyclic voltammetry [60].

Given a method to calculate the capacitance of each CV, we can now use it as a predictor of the electrode's condition. We then hypothesized that adding a mixed monolayer of aptamer backfilled with MCH would decrease the amount of current able to

pass through the system and thus decrease the capacitance. A decrease results because the monolayer hinders electron transfer. Then, when exposed to E2, we would expect an increase in capacitance and current. When the aptamer is exposed to E2, it will cause the aptamer to fold. That folding will bring the negatively charged backbone of the aptamer closer to the electrode's surface, resulting in an increase of electron transfer. We expect that the change in capacitance is positively and proportionally correlated to the concentration of E2. As more E2 is exposed to the surface, more of the aptamers should fold.

Table 3.3: Capacitance equations' variables

Symbol	Value	Physical Meaning
dE/dt	50mV/s	Voltage scan rate of the potentiostat
C	-	Capacitance
I	-	Current
A	$3.14x10^{-4}$ mm	Surface area of the working electrode
B	-	Capacitance over surface area

3.2.3 Cleaning Procedure

All materials in the system were cleaned before experimentation with ultrapure deionized water (DI). However, a specific polishing procedure is required for the working electrode to ensure repeatable results. The working electrode is the aptamer immobilization surface and site of the redox reaction, so any extraneous debris will greatly impact the resulting signal. Note that there may still be scratches on the surface of the working electrode. A properly cleaned surface should look reflective. Figure 3.6 shows the gold working electrode prior to cleaning, and after the cleaning protocol has been performed.

The following procedure has manual polishing with alumina slurry intermittent with sonication. This is because the alumina is abrasive enough to clean the electrode surface without damaging it, but it must be sonicated after to eliminate alumina particles from becoming compacted into the gold polishing surface. Otherwise, the alumina may catalyze the behavior of hexacynoferrate.

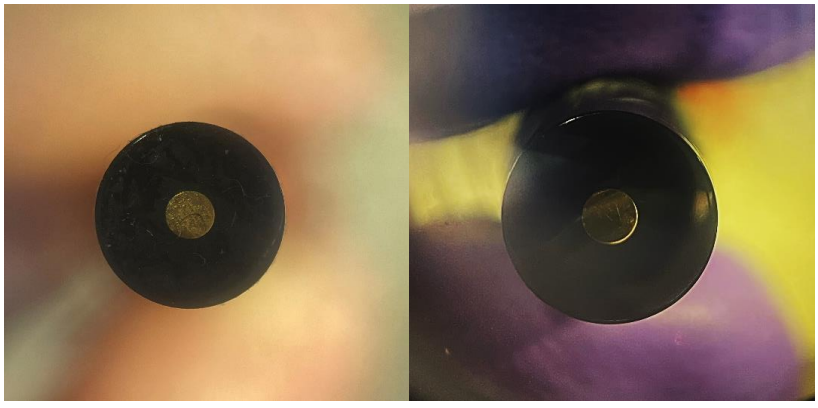

Figure 3.6: Gold working electrode prior to cleaning procedure (left), and after cleaning procedure (right).

However, by polishing with alumina, there is the risk of high background current originating from trace alumina, impurities, or adsorbed layers of hydroxy radicals [62].

The following steps were performed and are collectively referred to as the "Electrode Cleaning Protocol". The term "echem" is short for electrochemistry.

1. Clean all glassware and setup echem station.
    a. Rinse glassware with DI, then gently wash with condor soap, rinse three more times with DI or until there are no suds left.
    b. Follow "Echem Station Setup Protocol" in the next section.
2. Cut felt polishing pads into three 4in radius quadrants and stick to glass plate.
3. Take approximately 1 gram aliquots of 1 micron, 0.3 micron, and 0.05 micron alumina grit and place in separate 20mL glass containers.
4. Add DI to each aliquot's glass container until a viscous slurry is formed.
5. Pipette the 1micron slurry onto a felt pad.
    a. It is recommended that you do not pipette the slurry onto the felt pad until it is immediately ready for use, to prevent it from drying out.
    b. If slurry dries or becomes too viscous, add DI.
    c. A Pasteur pipet and bulb were used to pipette in this step.
6. Grind the working electrode in a figure-8 motion for 10 minutes.
7. Rinse with DI.
8. Sonicate for 5 minutes.
9. Rince with DI.
10. Sonicate for 5 minutes.
11. Move to the next smallest grit and repeat steps 5-10 until all three grits are used.

12. Perform cyclic voltammetry using 1M sulfuric acid, for setup procedures, follow EChem Setup Protocol.
    a. Initial E (V) = 0.4
    b. High E (V) = 1.8
    c. Low E (V) = 0.2
    d. Scan Rate (V/s) = 0.05
    e. Segment = 100
    f. Sensitivity (A/V) = 1e-5
13. Rinse with DI.
14. Electrode is ready for use. Store the working electrode in a dry, closed container.

3.2.4 Aptamer Immobilization Protocol

In order for the aptamer to serve as a sensing mechanism, it must be immobilized onto the working electrode's surface. The working electrode is gold, so we are able to take advantage of thiol bonding in the immobilization process. This protocol immobilizes a single-stranded, DNA, estradiol aptamer on the surface of a standard gold working electrode. The aptamer is backfilled with MCH to allow room for folding.

This protocol is divided into two sections: General Procedures and Aptamer Solution Procedures. Collectively, these steps are referred to as the "Immobilization Protocol".

<u>General Procedures adopted and modified from Keighley, 2007 [61].</u>

1. Perform Electrode Cleaning Protocol.

    a. To obtain a “Bare Gold” voltammogram trace, that should be taken now. After that trace is taken, rinse with DI.

2. Expose working electrode surface to 25 µL of aptamer solution for 16 hours in humidity chamber.
    a. See the Aptamer Solution Procedures and Humidity Chamber sections below.
3. Rinse working electrode in immobilization buffer, TE.
4. Immerse working electrode in 1mM MCH for 1 hour.
5. Rinse working electrode in DI.
6. Perform cyclic voltammetry.
    a. Follow the EChem Station Setup Protocol.
    b. This is the mixed monolayer (MML) CV. If you do not want an E2-exposed CV, stop here and store in dry, closed container.
7. Rinse working electrode in DI.
8. Expose working electrode to desired E2 concentration for 30 minutes.
9. Rinse working electrode in DI.
10. Store in dry, closed container.

There are multiple modifications from Keighley, 2007. First, the General Procedure’s cleaning protocol covers four of Keighley’s steps: sonication, cyclic voltammetry, DI rinse, and dry with nitrogen. Next, Keighley’s protocol calls for rinsing with immobilization buffer and phosphate buffers varying in molarity. We omitted the latter step as we determined it was redundant for our purposes.

Aptamer Solution Procedures adopted and modified

from Henri, 2019 folding procedures [65].

Experimental:

1. Fold aptamer
    a. Take 21.7µL of stock aptamer and add 78.3 µL of TE buffer.
    b. Heat aptamer for 85°C for 5 minutes in hot bath.
    c. Incubate at room temperature for 15 minutes.
    d. Take 50µL for final solution.
2. Dilution Series for MCH
    a. Take 10µL of stock MCH (**A**) and add 990µL of TE buffer = **B**
    b. Take 10µL of **B** and add 990µL of TE buffer = **C**
    c. Take 23µL of **C** and add 77µL of TE buffer = **D**
    d. Take 50µL of **D** for final solution.
3. Add diluted MCH and aptamer. Mix using a vortex mixer for approximately 20 seconds.

The values specified in the steps above come from the computational steps below to make a total of 100µL of total solution.

Computation:

1. Choose desired concentration of thiol solution, 0.1mM or 100µM.

$$[thiol] = [aptamer] + [MCH]$$

2. Using chosen ratio of aptamer to MCH,1:10, find concentration of each part.

$$1 + 10 = 11\ parts\ total$$

$$\frac{100\mu M}{11} = 9.09\mu M \; one\; part\; concentration$$

Multiply one part concentration by number of parts of each solute.

$$Aptamer: 1 * 9.09\mu M = 9.09\mu M$$
$$MCH: 10 * 9.09\mu M = 90.09\mu M$$

3. Now find the volume of aptamer and MCH needed.

$$Aptamer: v_1 = \frac{c_2 v_2}{c_1} = \frac{(9 * 10^{-6}) * (100 * 10^{-6})}{8.3 * 10^{-5}} = 10.8\mu L \approx 11\mu L$$

$$MCH: v_1 = \frac{c_2 v_2}{c_1} = \frac{(90 * 10^{-6}) * (100 * 10^{-6})}{7.8} = 1.15nL$$

$8.3x10^{-5}$ M is calculated from 298nM in 3mL of aptamer solution.

The final solution is 1.15nL of 90 µM MCH (0.00115 µL) combined with 10.8 µL of 18 µM aptamer with 89.19885 µL of TE buffer for a total of 100 µL of solution. We decided to make this solution by dividing it into two 50 µL solutions. We will be using 50 µL of 18µM aptamer and TE buffer and combining it with 50 µL of 180µM MCH for a final aptamer concentration of .18M.

4. Determine necessary volumes for 1:2 dilution series of aptamer.

$$c_1 = \frac{c_2 v_2}{v_1} = \frac{(9\ \mu M) * (100\mu L)}{50\mu L} = 18\mu M$$

C_2: final aptamer concentration
V_2: final solution total
V_1: desired dilution ratio volume
C_1: needed concentration for desired volume

$$v_1 = \frac{c_2 v_2}{c_1} = \frac{(18\mu M) * (100\mu L)}{83\mu M} = 21.7\mu L$$

C_2: aptamer concentration determined above
V_2: TE + aptamer desired volume total
V_1: needed volume of initial aptamer stock
C_1: concentration of stock

5. Determine necessary volume for dilution series of MCH.

$$v_1 = \frac{c_2 v_2}{c_1} = \frac{(180\mu M) * (100\mu L)}{7.8\mu M} = 2.3nL$$

C_2: needed MCH concentration for desired volume
V_2: desired dilution ratio volume
V_1: needed initial stock of MCH
C_1: concentration of stock

Because 2.3nL cannot be reliably measured, a dilution series is needed. We start with a 10 µL measurement because it can be measured reliably and only a 10^4 dilution is needed.

A is 10 µL of stock = 7.8M

B needs a 1:100 dilution so 10 µL **A** + 990µL TE = 78mM

C needs a 1:100 dilution so 10 µL **B** + 990µL TE = 780µM

D needs 23/100 parts as determined above, so 23 µL **C** + 77µL TE = 180 µM

Humidity Chamber

Each electrode is suspended in a 20mL container, upside down, to keep the electrode surface in a humid environment, and free from contaminants. The three containers are placed inside of a large beaker lined with damp paper towels. Parafilm is placed over the top of the beaker, seen in Figure 3.7.

Figure 3.7: Humidity Chamber for estradiol DNA aptamer immobilization procedure. Parafilm covers the top of a beaker lined with damp paper towels. Inside, three electrodes are suspended in 20mL glass containers to stay protected against contaminants.

3.2.5 Cyclic Voltammetry Procedure

For a cyclic voltammetry experiment to take place, we must setup the aqueous electrochemistry cell (echem cell) and potentiostat. This procedure is referred to as "Echem Station Setup Protocol" and is the standard set of steps performed prior to each CV session using the standard gold electrodes:

1. Clean all glassware and electrodes following electrode cleaning protocol.
2. Turn on Potentiostat, CH Instruments 660B Potentiostat/Galvanostat.
3. Place aqueous echem cell in lab clamps to prevent it from touching the counter.
4. Fill echem cell with 30mL of electrolyte solution.
5. Rinse counter, working, and reference electrode. Place in separate openings of echem cell, ensuring that they do not touch, but are reasonably close to one another. Connect electrodes to the potentiostat's counter, working, and reference leads.

6. Put Pasteur pipet into small opening and attach it to a Nitrogen valve. Use parafilm to secure the pipet and prevent any leakages.
7. Open the nitrogen valve to purge. Ensure that the electrolyte is softly bubbling. Let purge for 30 minutes to 1 hour.
8. Open Echem Program CH 660B on the computer connected to the potentiostat. Go to Setup and select cyclic voltammetry. Exit. Go back to Setup and select Parameters. Input desired parameters.
9. After purging, raise the pipet out of the electrolyte solution, but not the echem cell. You may need to turn down the Nitrogen valve to ensure to ensure that the surface of the electrolyte solution is not being moved by the expulsion of the gas from the pipet. This will maintain a thin Nitrogen gas layer on the surface of the solution.
10. Check the surface of the working electrode to ensure there are no bubbles. If there are bubbles, use the Nitrogen pipet to blow them off before returning the pipet to above the electrolyte solution's surface.
11. Press play in Program.
12. Save trace as CSV file.

The electrolyte solution for the cyclic voltammetry is 1M KCl. We prepared a 50mL batch so the same molarity of solution could be used, limiting variability. For the electrode cleaning protocol, the electrolyte solution is 1M ferri/ferrocynide. A photo of the echem cell setup ready for experimentation is shown below in Figure 3.8.

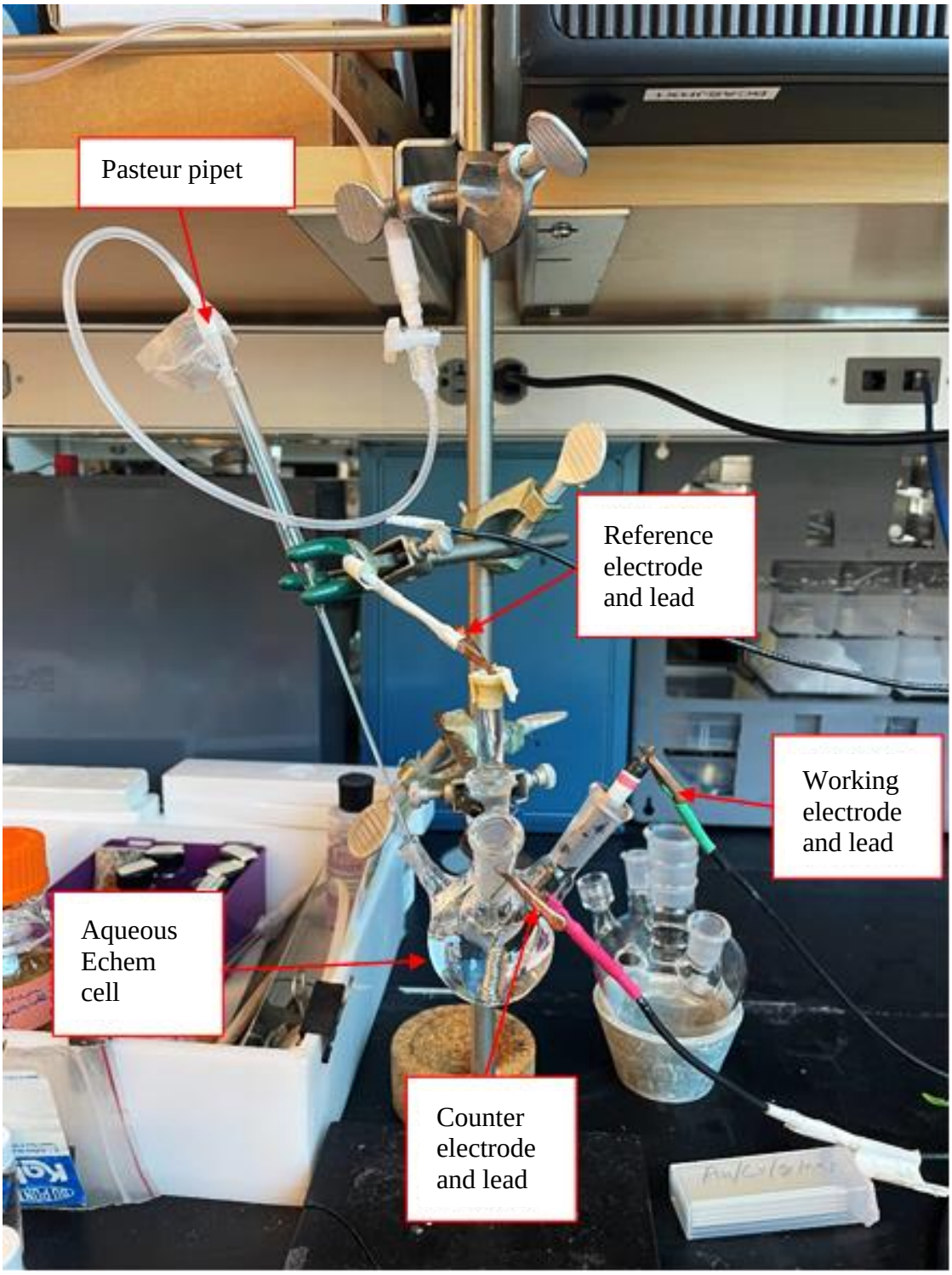

Figure 3.8: Echem cell final setup

3.2.6 Results and Discussion of Cyclic Voltammetry Experiments

In this section we will apply the aforementioned cyclic voltammetry principles to quantitatively determine the difference in the electrode conditions: bare gold, mixed monolayer, estradiol 10ng/mL, estradiol 100ng/mL, and estradiol 1000ng/mL. The capacitance of each CV was calculated and can now be used as a metric for comparison between electrode conditions. We expect the capacitance to decrease when the gold electrode goes from bare to mixed monolayer. However, when we expose the gold electrodes with the MML to different concentrations of estradiol, we expect a proportional increase in capacitance. Therefore, we have five states of the gold electrode's surface, summarized in Table 3.4.

The Bare Gold (BG) condition of the electrode is the state immediately after the cleaning procedure is performed in Section 3.2.3. After the CVs are taken for this condition, the Mixed Monolayer (MML) condition is created following the Aptamer Immobilization Protocol from Section 3.2.4. Once the CVs for the MML have been taken, the electrode is exposed for ten minutes to one of three estradiol concentrations: 10ng/mL, 100ng/mL, or 1000ng/mL. Forty total trials were conducted. However, six of those trials were discarded due to excessive noise or irregular shape. The criterion for data omission due to noise and irregular shape was described in Section 3.2.2. Therefore, the results of this study are based on the following 34 trials. Tables 3.6-3.10 summarize the 34 trials that were used for analysis in this report; the tables are separated by electrode condition and organize the data by electrode number and date of experimentation.

Table 3.4: Abbreviations and meaning of five electrode conditions analyzed in this study

Abbreviation	Meaning
BG	Bare Gold: the electrode is freshly cleaned, and nothing is on its surface
MML	Mixed Monolayer: the electrode has aptamers on its surface and is backfilled with MCH
E210	Estradiol 10ng/mL: the electrode has the mixed monolayer attached and has been exposed to 10ng/mL concentration of estradiol
E2100	Estradiol 100ng/mL: the electrode has the mixed monolayer attached and has been exposed to 100ng/mL concentration of estradiol
E21k	Estradiol 1000ng/mL: the electrode has the mixed monolayer attached and has been exposed to 1000ng/mL concentration of estradiol

Table 3.5: Legend for Tables 3.6-3.10 classifying usability of CVs

Symbol	Meaning
NA	Trial was not conducted
G	Good trial, acceptable shape and minimal noise
X1	Discarded trial, irregular shape
X2	Discarded trial, noisy
G*	Good trial, but an outlier

Table 3.6: Trials used for BG electrode condition

Date		Electrode	
	2	3	4
11.7.21	G	G	G
11.9.21	NA	NA	NA
11.10.21	NA	NA	NA
11.16.21	NA	NA	NA
11.23.21	NA	NA	NA
11.29.21	G	G	G

Table 3.7: Trials used for MML electrode condition

Date		Electrode	
	2	3	4
11.7.21	X1&X2	X1	X1&X2
11.9.21	G	X1	G
11.10.21	NA	NA	NA
11.16.21	G	G	G
11.23.21	NA	NA	G
11.29.21	X2	G*	G

Table 3.8: Trials used for E210 electrode condition

Date		Electrode	
	2	3	4
11.7.21	NA	NA	NA
11.9.21	G	X1&X2	G
11.10.21	G	G	G
11.16.21	NA	NA	NA
11.23.21	NA	NA	NA
11.29.21	NA	NA	NA

Table 3.9: Trials used for E2100 electrode condition

Date		Electrode	
	2	3	4
11.7.21	NA	NA	NA
11.9.21	NA	NA	NA
11.10.21	G	G	G
11.16.21	G	G	G
11.23.21	NA	NA	NA
11.29.21	NA	NA	NA

Table 3.10: Trials used for E21k electrode condition

Date		Electrode	
	2	3	4
11.7.21	NA	NA	NA
11.9.21	NA	NA	NA
11.10.21	NA	NA	NA
11.16.21	G	G	G
11.23.21	G	G	G
11.29.21	G	G	G

The trials from Tables 3.6-3.10 are classified by usability according to Table 3.5, below. Visualizations for these conditions can be found in Section 3.2.2. G* is not explicitly shown as it has the shape and noise-level of a good trial; however, its capacitance is greater than two standard deviations away from the mean when sorting by electrode condition. G* is included in the dataset unless explicitly stated otherwise.

Due to the nature of this exploratory study, we did not run a CV with every electrode condition each experimental day. We initially ran our tests with 10ng/mL estradiol, but did not see a relatively large capacitance response, so we began to use higher concentrations. We felt it was unnecessary to test lower concentrations on the later experimental days, seeing as how they did not provide an adequate capacitance response in our initial trials. Thus, there are gaps in the data where not all electrode conditions are tested each day.

There are three parameters we are testing: electrode condition, electrode number, and date of experimentation. This study demonstrates that the electrode condition is the most significant parameter in determining the capacitance of the system. Thus, electrode number and date are confounding factors that must be demonstrated to be less significant in influencing capacitance in order to demonstrate the utility of the sensing mechanism.

The boxplot in Figure 3.9 shows the results of all 34 trials sorted by electrode number. Electrode 2 has 11 data points, electrode 3 has 10 data points, and electrode 4 has 13 data points.

The median capacitance between the electrodes do not significantly differ. According to this boxplot, the capacitances of all of the electrodes are skewed to the high end. There are 5 outliers that are the result of the bare gold trials which are significantly different than the rest of the data. The spread of electrode three is slightly larger than electrodes two or four, but the median and lower limits are within 10μF/cm^2 so we can qualitatively observe that there is no significant difference in capacitance between the electrode numbers.

To determine if our other known confounding factor, date, was contributing to a change in capacitance, a time series was created. The time series accounts for day-to-day transient changes that might confound a change in capacitance. The time series has the

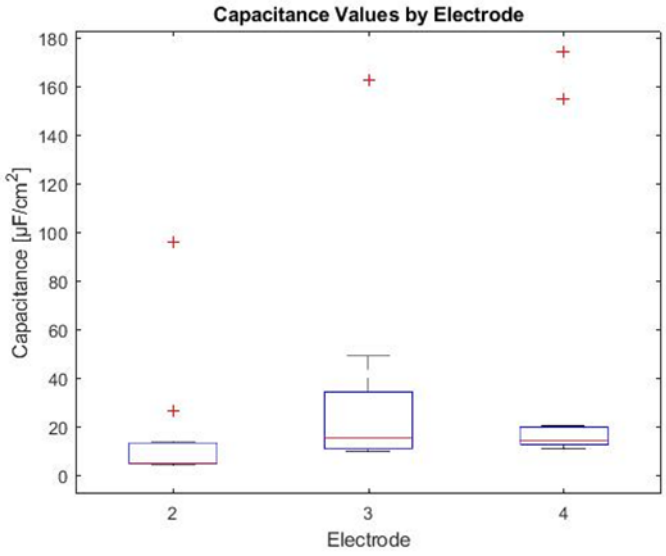

Figure 3.9: Boxplot of capacitances, separated by electrode

form of a scatter plot where each dot is a capacitance value from a trial, color coded by electrode condition. The x-axis is the days that the trials were conducted. Figure 3.10 excludes the irregularly shaped/noisy and bare gold trials.

Following the ‘MML’ and ‘E21k’ markers, there appears to be a slight upward trend as the month progresses. However, because of electrode condition and date being confounded, we must conduct a multi-factor ANOVAs to quantitatively determine the effect of the known parameters of electrode number, condition, and date of experimentation. The date and electrode condition are inherently correlated, so we will be unable to conclude that it has no effect. Similarly, the electrode condition and electrode number are inherently confounded since there is not an even number of usable trials for each electrode condition on each electrode. The ANOVA results rank the effects of the known parameters and demonstrate that electrode condition is the most significant in determining the capacitance of the system.

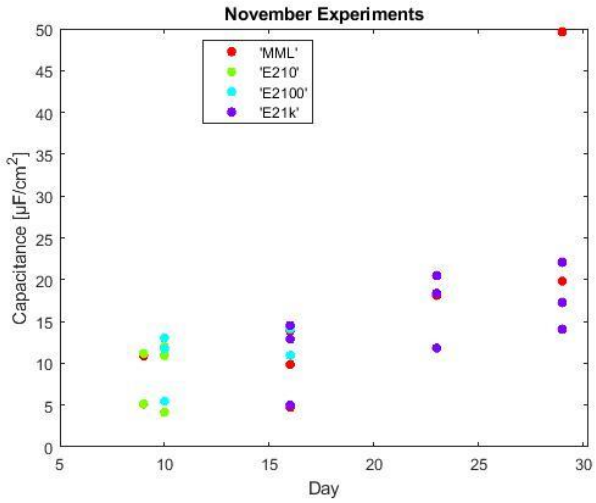

Figure 3.10. Time series excluding irregularly-shaped, noisy, and bare gold trials

We have reasoned that electrode condition and date of experimentation are two parameters influencing resulting capacitance when compared to electrode number and their respective interactions. A three-factor ANOVA is conducted between all parameters to rank their effects, summarized in Table 3.11.

When comparing the p-values from the three-factor ANOVA to a pre-determined alpha of 0.1, the following parameters are considered significant: electrode condition, date, electrode number, and the interaction between electrode condition and electrode number. This three factor ANOVA allows us to see that the electrode condition's p-value is multiple orders of magnitude smaller than the other statistically

Table 3.11: Three-factor ANOVA comparing electrode condition, data, and electrode number

Factor	DF	Sum Sq	Mean Sq	F value	P-Value
Electrode Condition	4	44729	11182	37.689	1.25E-5
Date	5	8653	1731	5.833	0.01128
Electrode Number	1	2987	2987	10.066	0.01132
Electrode Condition: Date	3	229	76	0.257	0.85428
Electrode Condition: Electrode Number	4	7879	1970	6.639	0.00901
Date:Electrode Number	5	852	170	0.574	0.71946
Electrode Condition: Date:Electrode Number	2	285	142	0.480	0.634
Residuals	9	2670	297		

significant parameters. Accordingly, the confounding parameters in order of increasing effect on capacitance are: interaction between electrode condition and electrode number, date, and electrode number. Therefore, while we cannot conclusively state that these parameters do not confound the resulting capacitance, we can assume that their effects are outweighed by that of the electrode condition.

We will further explore capacitance as a predictor of electrode condition, now that we have determined that electrode condition is the most significant parameter in determining capacitance. Figure 3.11 is a boxplot to compare the capacitances of the 34 trials specified in the introduction of this section, separated by electrode condition. The bare gold trials have the largest standard deviation and have capacitance values that are significantly larger than the other electrode conditions. However, because of its magnitude it is difficult to visualize the differences among the other electrode conditions. To better emphasize the differences between the added layers, Figure 3.12 excludes the bare gold trials. When the bare gold trials are excluded, there are some subtle differences between other electrode conditions. While it appears that the E210, E2100, and E21k layers are different from one another, the G* trial on the MML layer extends the y-axis, making it difficult to discern this. Figure 3.13 excludes the G* trial; after many trials, the spread and median would likely behave most closely to Figure 3.13.

Now that the bare gold and G* trials are omitted, we can more closely differentiate the behavior of the capacitances among the added layers. The size of the standard deviations among these layers appears to be similar. The minimum capacitance of all layers are within two $\mu F/cm^2$ and the median capacitance value is within six $\mu F/cm^2$.

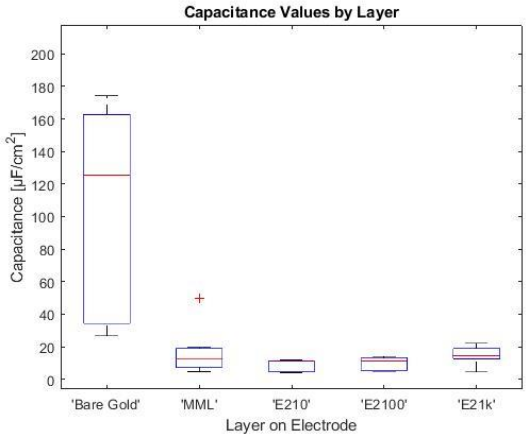

Figure 3.11: Boxplot of capacitance values separated by electrode condition

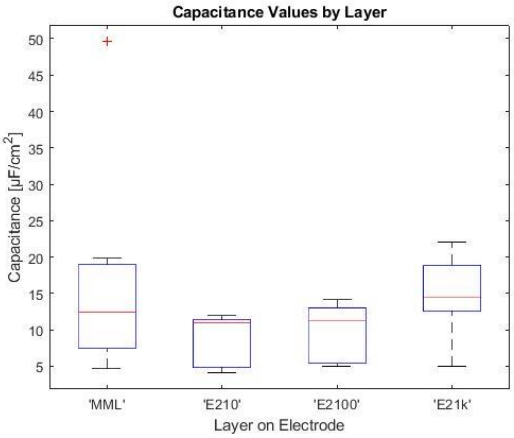

Figure 3.12 Boxplot of capacitance values separated by electrode condition, excluding BG

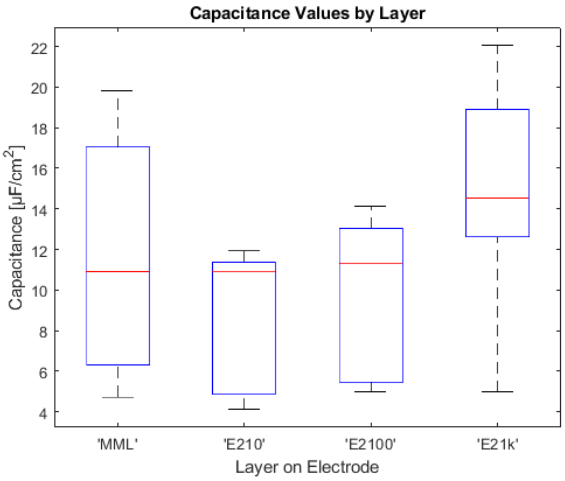

Figure 3.13 Boxplot of capacitance values separated by electrode condition, excluding BG and G*

We can visually determine that the maximum capacitance of each electrode condition is noticeably different. From this visualization, it is unclear what the extent of the differences are between the electrode conditions so we will explore further with summary statistics and single-factor ANOVAs.

A series of bar charts to compare the electrode conditions follows. Figure 3.14 compares the 34 trials' average capacitance by electrode condition.

The bare gold trials' averages are significantly higher than all other groups, and the difference between the added layers appears minimal. Similar to the boxplot above, we will remove the bare gold and G* trials to better visualize the differences among the added layers, Figure 3.15.

When the outlier, G*, is omitted from the data it follows a pattern that we would expect: capacitance increases with the concentration of estradiol. The effect of this outlier is emphasized in Figure 3.16, where (a) shows the standard deviation with the outlier, and (b) shows the standard deviation without the outlier.

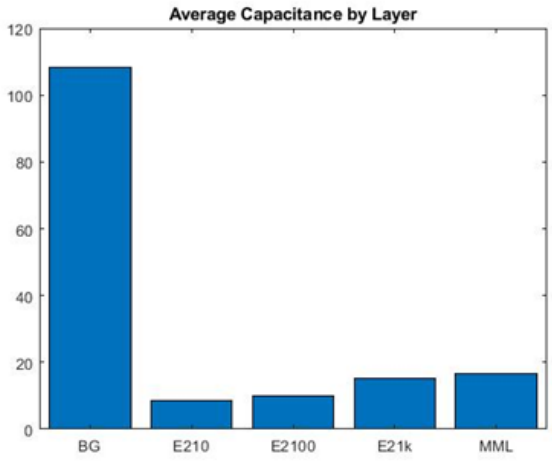

Figure 3.14: Bar chart of average capacitance values by layer

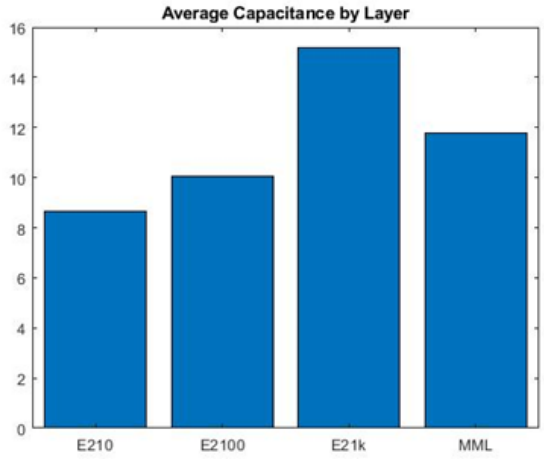

Figure 3.15 Bar chart of average capacitance values by layer excluding BG and G* trials

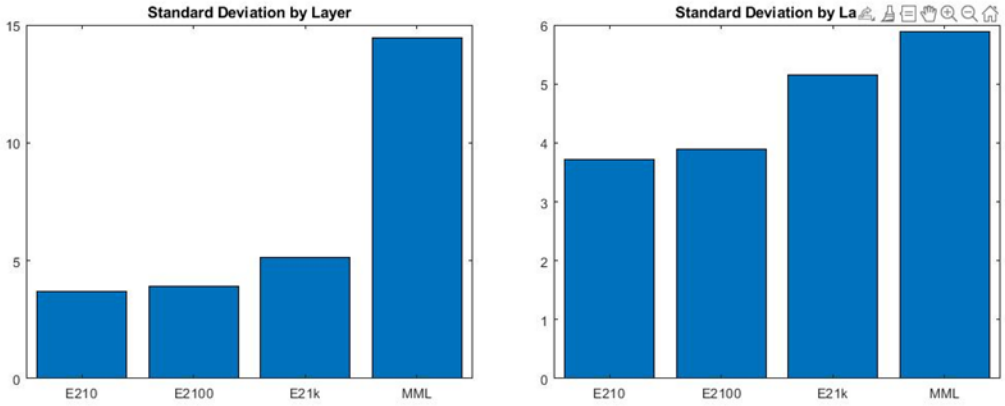

Figure 3.16: Standard deviation of added layers. (a) Left, includes all data. (b) Right, excludes G* trial

As was inferred from the boxplot, the standard deviations among the electrode conditions are relatively similar. Therefore, the noise among each added layer is approximately the same. This corroborates that our experimental procedures are likely consistent between groups and the transient confounding factors have approximately the same effect on each added layer. However, it is evident that the G* trial has a significant

effect on the MML's standard deviation. Table 3.12 organizes the electrode conditions' summary statistics from the visualizations above in $\mu F/cm^2$.

The mean capacitance increases with the concentration of estradiol. The mean difference between the average capacitances of the estradiol conditions is about 3.25 $\mu F/cm^2$. From Table 3.12, it is evident that the maximum capacitance value has the largest difference between electrode conditions.

To test if there is a difference between the electrode conditions, a single-factor ANOVA between all five electrode conditions was conducted (See Table 3.13). Based off of the initial boxplot, Figure 3.9, it is unsurprising that the ANOVA indicates a significant difference between the electrode conditions. To ensure that this difference is not solely from the bare gold trials, we conduct another single-factor ANOVA that omits the bare gold condition capacitance values. Table 3.14 is the summary of that single-factor ANOVA.

Table 3.12: Basic statistical summary based on electrode condition in $\mu F/cm^2$

Electrode Condition	Mean Capacitance	Min Capacitance	Max Capacitance	Standard Deviation
BG	108.1	26.66	174.3	65.96
MML	16.50	4.72	49.62	14.45
E210	8.66	4.13	11.96	3.72
E2100	10.04	4.99	14.13	3.89
E21k	15.16	4.98	22.05	5.15

Table 3.13: Single-factor ANOVA between five electrode conditions

Factor	DF	Sum Sq	Mean Sq	F value	P-Value
Electrode Condition	4	44729	11182	13.77	2.08E-6
Residuals	29	23554	812	-	-
Total	33	68283	-	-	-

Table 3.14: Single-factor ANOVA between MML and E2 concentration groups

Factor	DF	Sum Sq	Mean Sq	F value	P-Value
Electrode Condition	3	284.4	95.79	1.261	0.31
Residuals	24	1803.8	75.16	-	-
Total	27	511.5	-	-	-

From this second ANOVA, we can immediately realize that the main difference between electrode condition groups exists due to the bare gold trials. A series of t-tests were conducted to further investigate what differences exist between electrode conditions.

The series of post-hoc t-tests between means are to determine which electrode conditions have mean capacitance values that are statistically significant. A p-value less than 0.1 indicates that the electrode conditions have unequal means, thus there may be a difference in mean capacitance values between groups. The six t-tests and their results are detailed in Table 3.15.

The estradiol concentration level conditions are statistically significantly

Table 3.15: Results of post-hoc t-tests between two means for electrode conditions, excluding BG

Group 1	Group 2	P-Value
MML	E21k	0.797
MML	E2100	0.3113
MML	E210	0.2661
MML	BG	0.0023
E21k	E2100	0.0597
E21k	E210	0.0296
E2100	E210	0.5647

different according to our predetermined significance level, 0.1. We understand that by conducting multiple t-tests, there is an increase in likelihood of a type I error. A Bonferroni correction factor can be applied to alleviate this; for our t-tests it would result in an alpha of 0.016. By this standard, only the difference between MML and BG would be considered significant. However, it is evident that the other two highlighted cases have p-values that are an order of magnitude smaller than non-highlighted cases, so we will still consider them meaningful different despite not satisfying the Bonferroni alpha.

We can reasonably assume that the effect from the experimentation date and the electrode number is far less significant than that of the electrode condition. While these confounding factors and their interactions may play a role in the resulting capacitance values, we will assume that electrode condition is the primary indicator. Thus, our parameter of interest, electrode condition, was further explored as an explanatory variable for differing capacitance values.

It can be determined that there is a difference in mean capacitance between the bare gold surface and the mixed monolayer surface. Additionally, there is a clear positive correlation between estradiol concentration and average capacitance. Conversely, there is no evidence to suggest that there is an apparent difference between the mixed monolayer condition and any of the estradiol concentration conditions. Our hypothesis was that the MML would prevent the flow of current prior to estradiol exposure; however, that is not what we observed. Further experimentation should be conducted to alleviate the uncertainty presented by the lack of significant difference between the MML and E2 conditions. We determined that the primary differences between electrode conditions are bare gold and mixed monolayer, E2100 and E21k, and E210 and E21k. While they may

not satisfy the Bonferroni alpha it is evident that their respective p-values are an order of magnitude smaller than other electrode condition pairings. Therefore, in the sensor's current state we could likely sense a difference between varying estradiol concentrations.

3.3 Conclusion

The experimentation process requires a consistent electrode cleaning protocol, echem cell setup, and aptamer immobilization protocol. Variability from these procedures could lead to confounded results.

The electrode cleaning protocol consists of physical and chemical cleaning. This ensures that the electrode surface is free of debris, as well as any previous monolayer, or estradiol. The steps of this protocol were adapted from Keighley, 2007 [61].

The echem station setup protocol connects the aqueous echem cell to the potentiostat, allowing us to obtain the necessary data from the experiment. This procedure should be executed before any CV is recorded.

The aptamer immobilization protocol contains the experimental procedure for adding a mixed monolayer with its computational reasoning. A summary of the necessary materials and their respective manufacturers can be found in Appendix B.

The purpose of the cyclic voltammetry experiments was to quantify the capacitive differences between the different electrode conditions. Due to the nature of an exploratory study, the dataset confounds the date and the electrode condition. However, we can determine that electrode condition is the most significant effect in determining capacitance among the factors: date, electrode condition, and electrode number.

According to the single and multi-factor ANOVAs, the capacitance of the

estradiol-exposed conditions increases with the concentration of estradiol. This behaves as we predicted: more estradiol means more aptamers are folding, bringing a stronger negative charge to the surface of the electrode and allowing more current to flow.

CHAPTER 4

DISSOCIATION AND REUSABILITY

Popular aptamer-based diagnostic tools available are single-use only. Rapid saliva COVID-19 tests are an apropos example in 2022 of a widely used aptamer-based single-use diagnostic tool [66]. Not only do they create excess waste because tests cannot be reused, but they are also unable to take continuous measurements. Implantation of a sensor of this nature would be futile. While reusable testing may not be as relevant during a global pandemic, continuous monitoring of biometric data could lead to better insight about an individual's overall health without the need for taking multiple blood draws and other biosamples.

4.1 Define Dissociation and Reusability

For our purposes, reusability is the ability of our sensor to take many continuous measurements for its implantation lifetime without any intervention from the user or physician. Ideally, a measurement would be taken every two hours for 30 days to provide enough information for a physician within a reasonable implantation period.

Association is the process of estradiol binding to the aptamer; conversely, dissociation is the process of estradiol leaving the aptamer. As previously detailed in Chapter 3, we expect binding to increase capacitance. If association and dissociation

continuously occur in vivo, the aptamer field will bind and release estradiol molecules proportionally to the concentration of estradiol in the body. Thus, the capacitance values cycle with the body's hormonal cycling due to the proportional association and dissociation of estradiol molecules to aptamers. Lag between the true estradiol level in the body and the reported estradiol level arises due to the association and dissociation rate.

The dissociation rate constant k_{off} and the association rate constant k_{on} depend on the local free energy maximum that separates the bound and unbound state of the aptamer [67]. K_D is the ratio of k_{off} to k_{on}, it is representative of the equilibrium dissociation constant. Meaning that at a stoichiometric ratio of 1:1, equilibrium, K_D is a measure of the tendency of the aptamer-estradiol complex to dissociate.

The following experiment examines if the aptamers can dissociate without intervention. The goal was to determine if the aptamer-estradiol bonds will break on their own within a designated period, or if they are at least semi-permanent. If the process of attachment-dissociation-attachment is possible, then the sensor can be qualified as reusable.

4.2 Dissociation Experiment

The following section will cover the procedure for the dissociation experimental work. The cleaning protocol and CV setup are the same from Section 3. The experiment took place over the course of two days: Day 1's session lasted 3.5 hours, and Day 2's session lasted 4.5 hours. CVs were taken every half hour.

Dissociation Experimental Procedure

1. Prep: Clean all materials using the Electrode Cleaning Protocol, and setup potentiostat according to the EChem Station Setup Protocol. Attach the MML using the Aptamer Immobilization Protocol and expose it to desired estradiol concentration for 10 minutes.
2. Take initial CV of all electrodes in 1M KCl.
3. Place each electrode in 10mL of 1M KCl for thirty minutes.
4. Rinse with DI water.
5. Take new CV of all electrodes in 1M KCl.
6. Rinse with DI water.
7. Repeat steps 3-6 as desired, replacing the KCl with a fresh sample after each CV.

4.3 Results and Discussion of Dissociation Experiment

In vivo, there will likely never be a 0ng/mL concentration of estradiol; accordingly, we would not expect the live capacitance to ever return to its MML value completely. As the estradiol of the individual rises and falls within a 24-hour period, the capacitance of the system follows a similar pattern. However, because there is a delay in response due to dissociation rates, there is a lag between the body's true estradiol level and the reported estradiol level which is determined by the capacitance value.

In order to find the dissociation lag time, we need to find the amount of time for most of the estradiol to completely dissociate from the aptamers. The experiment outlined previously (see Section 4.2), aims to do this by taking an electrode with an MML that has been exposed to 1000ng/mL of estradiol, and letting it sit in pure 1M KCl. Letting it sit in its electrolyte solution, prevents the aptamers from re-associating with estradiol.

Association and dissociation are spontaneous processes that, due to their relationships with binding affinity, are driven by the amount of free energy in the system. These concepts are expanded upon later in this Chapter. Thus, the process of dissociation is reflected by a decrease in capacitance.

Figure 4.1 shows the results of the dissociation experiment; it is a line plot of the capacitance of all three electrodes over an 8 hour time interval.

We arbitrarily chose an 8 hour time interval because we assumed it would be a long enough period to capture dissociation. The dashed line represents the 12 hour break between the last sample taken on Day 1 of experimentation and the first sample taken on Day 2 of experimentation. At time t=0 the electrodes' condition is E21k: the mixed monolayer creation and estradiol exposure occurred 33 days prior to dissociation experimentation. The last CV taken on Day 1 should have been nearly equal to the first CV on Day 2 since the electrodes were stored in a closed, dry container and no other treatments were imposed on the electrodes in between CVs. Only electrode 3 has

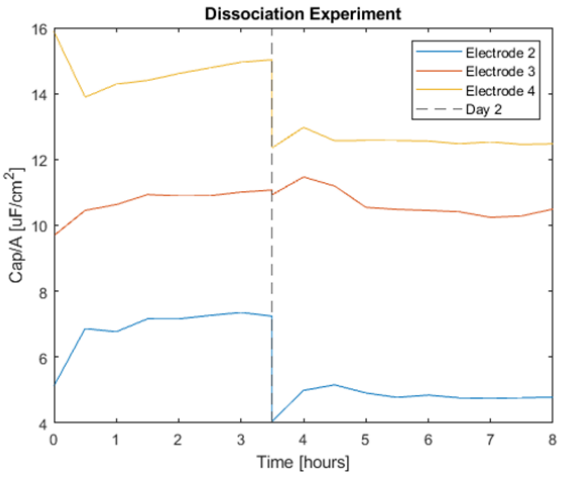

Figure 4.1: Capacitance over time for all three electrodes, sampling every 0.5 hours.

an acceptable step between experimentation days; it is unclear what transient factors caused the jumps in capacitance occurring at the same time for electrodes 2 and 4.

From Figure 4.1, the electrodes' capacitance values do not overlap, but this is expected. The average capacitance values of each electrode from Chapter 3 are slightly different and increase with electrode number. Therefore, we look at the spread of each electrode from Figure 4.1 to confirm reproducibility. Electrode 3's spread is about half that of the other electrodes, which is due to the minimal change in capacitance at the Day 1 to 2 break. Regardless, the spread is relatively inconsistent.

The largest changes in capacitance for each trace occurs within 1.5 hours from the start of the first CV of the day. It is unclear why the second CV taken each day increases in capacitance, with the exception of electrode 4 Day 1. It appears that equilibrium begins to be achieved after 1.5 hours each day.

It is difficult to conclude that dissociation is occurring within this time frame as the capacitance values are inconsistent and do not behave as expected. It should be noted, each electrode was exposed to estradiol 33 days prior to this experiment starting. We assumed that the age of the MML was negligible as the electrodes had been untouched, and stored in a dry, closed container. However, we can see from the dissociation experiment that despite these storage conditions, time in storage appears to influence capacitance. Figure 4.2 expands Figure 4.1 by including the capacitance value from the last CV taken on the day the MML was formed and exposed to estradiol (33 days prior).

The initial capacitance value from Day 1 of the dissociation experiment was expected to be the same as the capacitance value from the last CV taken on the day the MML was formed, and the electrodes were exposed to 1000ng/mL estradiol. The

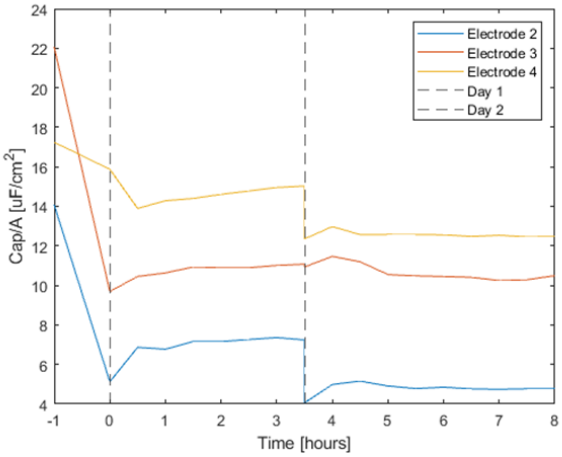

Figure 4.2: Dissociation experiment time trace, including capacitance value from the last CV taken on day of MML creation and E21k exposure.

difference in capacitance between the electrodes' capacitance values at time -1 and 0 is larger than traces' range. Therefore, we cannot conclude that our experiment captured any of the dissociation behavior, as it may have occurred prior to the start of the experiment.

4.4 Discussion of Theoretical Association and Dissociation

Despite being unable to capture the dissociation experimentally, we can approximate the dissociation and association response using a theoretical diurnal cycle. The diurnal cycle used for this theoretical exploration is developed using equation 4.1, developed by Bao et al. [35].

$$T(t) = M + A\cos[(t-\phi_1) + v\sin(t-\phi_1)] + B\cos(ut-\phi_2) \quad (4.1)$$

The study conducted by Bao et al. determined that the best-fit model for the diurnal fluctuations of free-estradiol, T(t), is a peaked cosine function with an additional harmonic ($P<0.10$ or better in 53 cases). Table 4.1 lists the variables, their meaning and values used for equation 4.1.

Table 4.1: Variables for equation 4.1

Symbol	Definition	Value
T(t)	Resulting concentration of free estradiol	-
t	Time of day in radians	n=100 array between 0 and 6.2832 rad
M	Mean 24 hour estradiol level	0.029368nM
A	Amplitude of diurnal component	0.0154182nM
Φ_1	Phase angle of diurnal component	2.45 rad
v	Peakedness	0.785rad
B	Amplitude of ultradian component	0.011013nM
Φ_2	Phase angle of ultradian component	-2rad
u	Constant for harmonic ultradian rhythm of 6 hours	4

The time of day, phase angles, and peakedness values had to be converted into units of radians to satisfy the equation. The array *t* translates to a 24-hour interval. The values for M, A, and B were taken from an example from the Bao et al. study, and converted into units of nM. The value for *v* is for a 3-hour peak. The value for *u* provides a 6-hour rhythm. The phase angles, and the harmonic constant *u*, were arbitrarily chosen to create a diurnal cycle that mimicked the cycle pictured in see Figure 4.3. Figure 4.3 shows the best-fit lines with experimental data developed by Bao et al. Figure 4.4 shows the theoretical cycle that we developed using equation 4.1 and the values from Table 4.1.

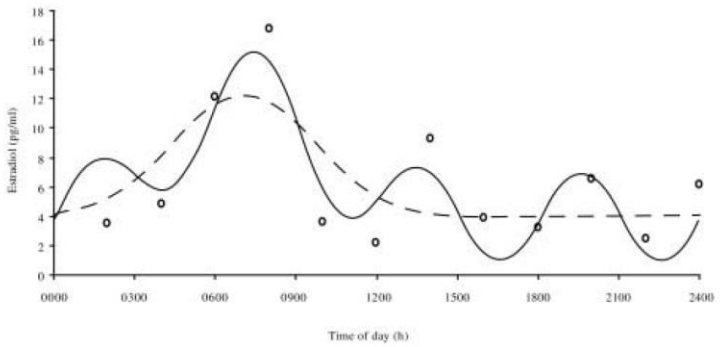

Figure 4.3: Subject no.11, phase III from Bao et al. Raw data points (circles) with full best-fit model (solid line), and peaked cosine 24-hour rhythmic component (dashed line).

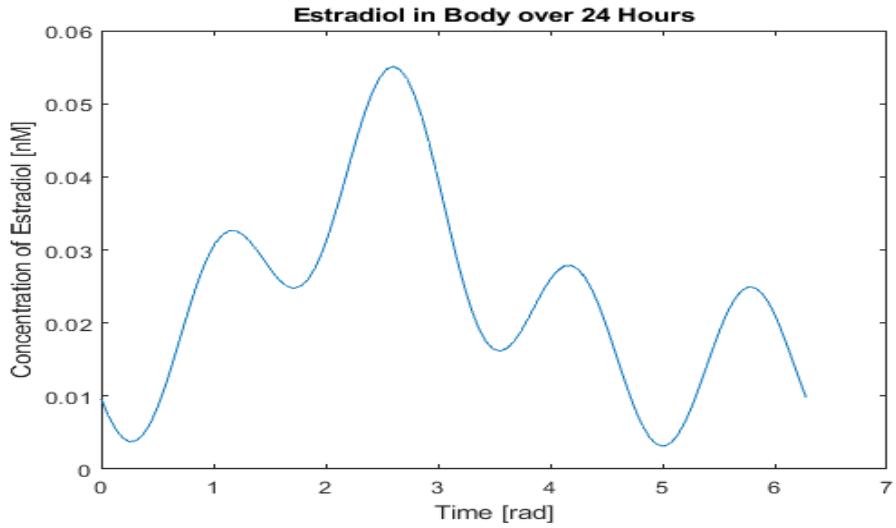

Figure 4.4: Theoretical diurnal cycle of free estradiol.

The exact values used for the curve in Figure 4.3 were not explicitly listed, so we approximated a curve, Figure 4.4.The parameters for Figure 4.4 were adjusted to closely resemble the components of the diurnal cycle in Figure 4.3. We ensured that the estradiol peak occurred between 0600 and 0900 hours, which translates to approximately 2 and 3 radians. Additionally, we wanted the harmonic to have three peaks that did not exceed the amplitude of the day's peak between 0600 and 0900 hours. Because Figure 4.4 is representative of a hypothetical, normal, diurnal estradiol fluctuation, we can assume that it is a reasonable representation to model the theoretical association and dissociation response.

In order to model the association and dissociation, we must first make a few assumptions. First, we are assuming that the sensor is acting as an equilibrium sensor in which the stoichiometry for the association and dissociation events is 1:1. Second, we assume that the total concentration of aptamer, is fixed and conserved. This is reasonable when modelling an implantable sensor that would be incapable of having aptamer

replenished. Next, we must assume that we can scale the diurnal cycle from Figure 4.4 to be representative of the fraction of bound aptamers. Meaning that we are translating the maximum and minimum estradiol concentration, in nM, to be equal to 1 and 0, respectively. This assumes that at the maximum estradiol concentration of the day, all the aptamers are bound, and at the minimum estradiol concentration of the day, none of the aptamers are bound. While this will never be possible with a non-gated equilibrium sensor in vivo, it is reasonable for the theoretical model. We are able to reason this scaling because the capacitance of the system is directly proportional to the amount of bound aptamers. Equation 4.2 describes the fraction of bound aptamers, at equilibrium.

$$f = \frac{[T]}{[T]+K_D} \tag{4.2}$$

[T] is representative of the concentration of free estradiol, and K_D is the equilibrium dissociation constant. Equation 4.3 is representative of the system acting in equilibrium where [A] represents the concentration of aptamer, and [AT] is the concentration of the aptamer-estradiol complex.

$$[A] + [T] \overset{k_{on}/k_{off}}{\longleftrightarrow} [AT] \tag{4.3}$$

K_{on} is the association rate; it represents the arrow going right with the complex forming. K_{off} is the dissociation rate; it represents the arrow going left with the complex separating. The process of association and dissociation is spontaneous, and can be viewed as a change in free energy. Free energy (ΔG) is the driving force of the formation of the AT complex, defined by the difference between enthalpy (ΔH) and entropy (ΔS). Equation 4.4 describes the change in free energy given a temperature T.

$$\Delta G = \Delta H - T\Delta S \tag{4.4}$$

When ΔG is negative, and the system reaches equilibrium at constant pressure and temperature, binding occurs. When ΔG is positive, there is a disruption of the energetically favorable bonds, causing dissociation. The net enthalpy change is a global property of the system, and can thus be convoluted by transient factors in the solvent. Equations 4.5 and 4.6 relate the Gibbs free energy of binding (ΔG°), the enthalpy of binding (ΔH°), the entropy of binding (ΔS°), the ideal gas constant (R) and the temperature in Kelvin (T) to the equilibrium dissociation constant (K_D).

$$\Delta G^{\circ} = -RT\ln\left(\frac{1}{K_D}\right) \tag{4.5}$$

$$\ln\left(\frac{1}{K_D}\right) = \frac{-\Delta H^{\circ}}{R} * \left(\frac{1}{T}\right) + \frac{\Delta S^{\circ}}{R} \tag{4.6}$$

Understanding how K_D influences the association and dissociation of the system from a thermodynamic perspective allows us to apply it in context of the fraction of bound aptamer. We do not have a K_D specific to our system, so we will use multiple different values to approximate the aptamer response: 0.045nM, 0.09nM, 0.009nM, and 0.0009nM. These values are on the order of K_D values of similarly sized complexes [68]. The lower the K_D value, the stronger the bond. Thus, lower K_D values are indicative of a high affinity in which the aptamer-estradiol complex are less frequently dissociating. The value of K_D is particular to the aptamer and can be determined through equilibrium dialysis, high-performance liquid chromatography, electrophoresis, fluorescence anisotropy etc.

Using our knowledge of the diurnal cycle and K_D, we can now model how the aptamers would associate and dissociate at the chosen K_D values, given the concentration of free estradiol. This model is shown in Figure 4.5.

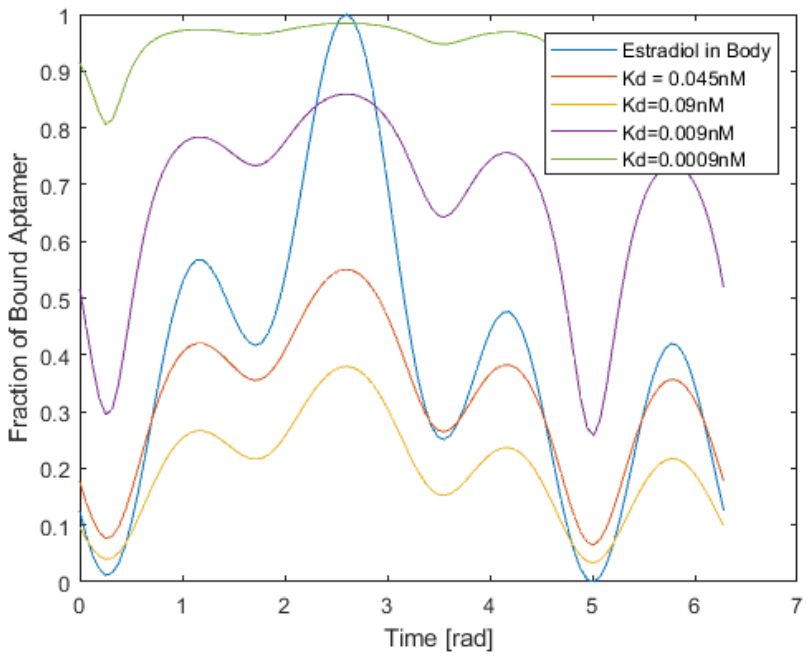

Figure 4.5: The diurnal fluctuation of estradiol in the body with various equilibrium dissociation constants, in units of fraction of bound aptamer.

The blue line represents the fluctuation of estradiol in the body scaled from 0 to 1 to represent the fraction of bound aptamers in the sensor throughout a 24 hour period. The orange, yellow, purple, and green curves represent the aptasensor's fraction of bound aptamers, at the listed dissociation equilibrium constants, given the concentration of estradiol in the body in nM. Knowing that the fraction of bound aptamer is directly proportional to the capacitance and reported estradiol, we can equate these curves as the reported estradiol response. As the value of K_D decreases, the aptamer's binding affinity for estradiol increase; therefore, a stronger bond is formed so more activation energy is required for the aptamers to dissociate. All of the curves capture the fluctuation of the diurnal cycle; however, the best approximation is the orange curve which uses an equilibrium dissociation value of 0.045nM, which had the lowest root-mean-squared

error among the theoretical curves (0.1544). This analysis showing the various K_D values influence on aptamer response could be useful when designing an aptamer for this application; an aptamer with very strong bonding capabilities or very weak bonding capabilities is not ideal.

4.5 Conclusion

Understanding the dissociation rate of the aptamers allows us to determine the efficacy of the sensor, and its ability to function as an implantable sensor. The ability of the aptamer to associate, dissociate, and re-associate means that the aptamer field is reusable, and can take multiple measurements without intervention. From experimentation, we were unable to determine if the sensor could be used continuously in vivo. Further experimentation would need to be conducted to determine if the aptamers used in this study are capable of dissociating, and doing so multiple times. Theoretically, an aptamer should be able to dissociate multiple times, the frequency of which is determined by the aptamer's binding affinity. From our theoretical analysis, if an equilibrium dissociation constant of approximately 0.045nM were achieved, we could adequately model the diurnal fluctuations in the body.

Once the sensor has been calibrated, we can translate a step in capacitance to a step in estradiol. Capacitance is dictated by the proportion of aptamers folding. The proportion of aptamers folding is reflective of the estradiol in the system. Therefore, as estradiol fluctuates throughout the day in vivo, so will capacitance. However, because the aptamers need to dissociate in order for a new estradiol level to be interpreted, a lag will

occur due to the rate of dissociation. The lag is between the true estradiol level in the body and the reported estradiol level, which is derived from the capacitance.

The lag is dependent on the strength of the aptamer's bonds. A very low K_D value implies a strong bond between aptamer and estradiol, which will decrease the frequency of dissociation. Conversely, a very high K_D value implies a weak bond between aptamer and estradiol, which will cause a frequency of dissociation so high that it may be difficult to capture the diurnal fluctuation. We were unable to determine a dissociation rate constants, which could be used to calculate K_D.

The dissociation experiment consisted of allowing all three electrodes to sit in 1M KCl over the course of two days for a total experimentation time of 8 hours. During the experimentation period, a CV was taken every thirty minutes. We hypothesized that we would see an exponential decrease from the first capacitance value to the last capacitance value. It appeared that after approximately two hours, each electrode reached equilibrium on both days. However, the electrodes' capacitance did not steadily, exponentially decrease. Except for electrode 4, Day 1, the second CV of the day for each electrode had a capacitance higher than the initial CV. The electrodes' behavior was inconsistent, which is why we cannot draw any conclusions from our experiment. We expected storage time to be negligible as all electrodes were all stored in a dry, closed container. However, we expect that the age of the MML and estradiol may have impaired the results.

CHAPTER 5

DISCUSSION AND CONCLUSIONS

5.1 Sensitivity and Limit of Detection

One of the challenges associated with creating an estradiol sensor is accommodating for the concentration range found in the body. An accurate estradiol sensor must be able to capture the diurnal and monthly cycle fluctuations. Quantitatively, these cycles normally range between 50pmol/L and 1,000pmol/L. An estradiol sensor should capture the normal range as well as abnormalities; therefore, it should ideally sense from a concentration of 10 pmol/L to 2,500 pmol/L. Values outside of this range would be considered abnormally low or high and indicative of other health risks [68]. Thus, the limit of detection must be 10pmol/L in order to capture abnormally low estradiol levels. From the Bao et al. study, the smallest step in concentration when sampling at 2-hour intervals over the diurnal cycle was 3.5pmol/L. Further, they determined that changes in concentration occurring at time intervals shorter than 2 hours were not meaningful. Thus, it is reasonable to conclude that the sensor's resolution should be 3.5pmol/L.

Other sensor specifications of importance include specificity, stability, and SNR. The specificity of the sensor is inherent due to the sensing mechanism, aptamers. However, the minimal drift and noise levels are not inherent to the system's design. For

the drift and noise to be considered negligible, they must both be smaller than our smallest step size in capacitance. Noise and drift can be caused by electrical interference and contamination which can be immanent to biological sensors [69].

We can evaluate the limit of detection and sensitivity requirements in its current state from our initial experiments. The smallest concentration of estradiol that we were able to reliably sense was 10ng/mL or 36,710pmol/L. Therefore, in the sensor's current state, we are unable to satisfy the limit of detection. We are also outside of the minimum and maximum requirements of the concentration range. The smallest concentration step that we were able to sense was from 10ng/mL to 100ng/mL, 90ng/mL or 330,390pmol/L. Therefore, the sensitivity is multiple orders of magnitude smaller than the required sensitivity.

Because we were able to detect different levels of estradiol, we can reasonably assume that the aptasensor is specific to its target molecule. Further experimentation would need to be conducted to quantify its specificity. Such an experiment could use the aptasensor in this study to measure the capacitance of a solution with estradiol and another hormone, like testosterone. The concentration of estradiol in the solution should have a known associated capacitance (1000ng/mL), and the concentration of testosterone would then vary. Then, one can determine how specific the system is by how much error results between the test solutions' capacitance and the known associated capacitance for the chosen estradiol concentration level.

A sensor's stability is dependent on the presence of drift. An experiment to determine drift and stability would consist of leaving the sensor in an electrode condition for an extended period of time and quantifying the change in measurement. However, the

sensor's ability to take consistent readings can be approximated using the standard deviation among the estradiol electrode conditions. For the E210, E2100, and E21k electrode conditions, the standard deviation is 3.72μF/cm^2, 3.89 μF/cm^2, and 5.15μF/cm^2 respectively. If we assume that the standard deviations among the estradiol electrode conditions can be averaged to represent the sensor's consistency, we get an overall standard deviation of 4.25μF/cm^2. Meaning that while we did not explicitly define stability, we know that our data is relatively consistent within 5 μF/cm^2. The SNR of every trial was determined visually, trials that did not satisfy the CV quality limitations established in Chapter 3.2.2 were discarded. These standards are evaluated qualitatively. We determined that if the band of the CV looked wide or fuzzy, then there was too much noise for the CV to be included in the data.

Before its design is modified for implantation, the sensor's sensitivity must be improved upon to meet the implantation requirements, given that it fails to meet these standards in its current state. However, the standard deviations of the estradiol electrode conditions' capacitances are low comparatively to their mean capacitances. This implies that the system can currently differentiate between the concentration levels used in this study, but that sensitivity is not high enough for implantation. Further testing would need to be conducted to quantify the selectivity of the sensor; but, we can reasonably assume it has satisfactory selectivity due to our results positively correlating concentration of estradiol and capacitance and the inherent specificity of aptamers.

5.2 Implantability

From a clinical perspective, the sensor needs to take samples over the course of 24 hours to provide useful, and relevant information for a user. Ideally, a sample would be taken every two hours. This means the association and dissociation must take place over the course of 24 hours without cleaning or replenishing of materials. From theory, we estimate that the frequency of dissociation and association will depend on the aptamer's binding affinity. The binding affinity will dictate the equilibrium dissociation constant, which we used to model the expected response given a diurnal cycle. However, further experimentation would need to be conducted to determine the equilibrium dissociation constant value through equilibrium dialysis, electrophoresis etc. Then the sensor's theoretical model could be better suited for comparison against an in vivo trial. The age of the MML or day of E2 exposure prior to the start date of the dissociation experiment likely confounded the results that could have informed us on the rate of dissociation. For best results in future work, the dissociation experiment should be reconducted on the same day in which the electrode's MML is formed and is exposed to estradiol.

For the sensor to last an implant lifetime of one month and take samples every two hours, the sensor needs to take 360 samples. If a more complex microfluidic chip is employed, then the aptamers themselves would have to withstand 360 exposures to biological fluid. However, if the aptamers are exposed to the biological fluid without any filtration or gate, they must be able to associate and dissociate in constant exposure. This capability was not evaluated in our study.

To determine the lifetime of the aptamers, first the association and dissociation time constants would need to be determined experimentally. If no modifications need to be done to the sensing mechanism to improve upon the association and dissociation rates, then an experiment evaluating the reusability of the sensor could be conducted. Such an experiment would determine if the aptamers can associate and dissociate during 360 exposures of biological fluid to accommodate a microfluidic gated system: give the sensor the necessary amount of time to reach equilibrium, changing the estradiol concentration incrementally and flushing with buffer solution in between different concentrations. This process should be repeated until the sensor reports capacitance values outside of what would be an acceptable error, or reaches 360 exposures, whichever comes first. If the total number of exposures is between 340 and 360, then the sensor can likely still be useful for a clinician. If the total number of exposures is between 200 and 340, then the clinical application should be reevaluated. Depending on the user's normal menstrual cycle duration and the clinician's desire to target a certain portion of the menstrual cycle, the device would be useful without any modification. However, if the total number of exposures is below 200, this is unsatisfactory. At this limit the sensor would not be able to continually sense for more than 17 days. A sub-17-day time frame is not wide enough to completely evaluate more than one phase of the user's menstrual cycle. The inability to capture more than one phase negates the benefits of continuous monitoring. The estradiol levels can vary widely from subject to subject and should be interpreted and contextualized through the lens of the entire cycle. With a sub-17-day lifetime, the sensor would have to be replaced to achieve this goal. Modifications must be made to the device if the sensor cannot last more than 200 exposures. Modifications

include increasing the surface concentration of aptamer or using a different kind of bio-receptor in place of an aptamer.

The ability for the sensor to function in constant exposure can be evaluated in a similar method, except that no buffer solution should be used and time should be the metric by which the sensor is evaluated. If continuous exposure causes inaccurate reporting or a shorter aptamer lifetime due to denaturation, then a gated microfluidic chip should be explored.

In its current state, the aptasensor is a benchtop setup. Including the potentiostat, the sensor takes up approximately $8ft^3$ or $2.26x10^8mm^3$. The CHI 660B Potentiostat used in this study uses a standard wall socket for its power supply, likely using about 15A at 120V. Evidently, both the size of the sensor and the power it currently uses is many orders of magnitude larger than what would be required for an implantable.

Using the Eversense glucose sensor as a template for an upper-arm implant, the sensor should be about 18mm in length with a diameter no larger than 4mm. The Eversense transmitter consumes 0.3-0.15A to supply its sensor with power. It is unclear exactly how much power the sensor receives from its transmitter. For our sensor's purposes, the sensor must include a battery that could supply the necessary power for the sensor's lifetime. If the sensor is intravaginal, its design could accommodate a larger volume, and thus a larger battery which could extend its implantability lifetime.

5.3 Limitations

Like all biological sensors, an estradiol sensor's readings could be convoluted by the influence of other biological material. The false reporting of a sensor due to

convolution of non-target biological molecules is called biofouling. Aptamers are used due to their high specificity to target molecules but can still be susceptible to biofouling. The high selectivity of the aptamer is unable to overcome the body's response to actively contain a foreign object; it is possible for the body's response to block the aptamers from sensing the environment. Further physical filtration could be added to the sensor to minimize the aptamers' contact with non-target molecules. Acceptable error from biofouling for clinical use would be roughly 10%. In context of reported estradiol levels, if the ideal sensitivity is 3.5pmol/L, then a 10% error would equate to 0.35pmol/L, which does not change the implications of the reading from a clinical perspective; however, further deviation from this value could give users or their health care providers a false understanding of the patient's estradiol levels.

1M KCl was the electrolyte the aptasensor was tested in. In vivo, either blood or cervical mucus would serve as the electrolyte for cyclic voltammetry. While KCl is neutral, biological fluids can vary in acidity. Thus, we do not know the potential accuracy of sensor given a slightly more basic or acidic electrolyte. Further work could include repeating the experiments of Chapter 3 with electrolytes varying in pH to determine if it has an effect on the folding characteristics of the aptamers.

If the sensor is to be implanted into the upper arm, its shape would likely be cylindrical, like the Nexplanon or Eversense. This shape is conducive for both implantation and removal. The cylindrical shape minimizes the amount of surface area for its given volume, compared to other shapes. Additionally, a cylinder can easily be rolled out from under the skin with a small incision. Other shapes like a rectangular prism are bulky and difficult to grip for extraction. If the sensor were to be intravaginal, then it

would be shaped similarly to a NuvaRing or the Layla Wellness PreOv ring. A ring shape maximizes the volume that the sensor can take up. Other shapes such as rectangular prisms or cylinders could get lost or stuck in the cervix or vaginal canal. Additionally, these shapes would likely cause discomfort as they do not conform to the natural shape of the vaginal canal.

5.4 Conclusion

The purpose of this research was to undertake an exploratory study of an electrochemical sensor for detecting estradiol with the eventual goal of continuous sampling and implantability. Fertility monitoring is important not only as a family planning tool, but as a health diagnostic. Current fertility monitoring solutions are based on assumptions as they are incapable of continuously monitoring the hormones that dictate the menstrual cycle itself. This inaccuracy can not only lead to an unwanted pregnancy but can make it extremely difficult for an individual to become pregnant. In addition to being inaccurate, current fertility awareness methods, such as the calendar method or cervical mucus method, are unable to detect if an individual has a fertility disorder or hormone imbalance. Diagnosis of a fertility disorder or hormone imbalance requires direct measurement of estradiol and other menstrual cycle predicting hormones in addition to other diagnostics. Paradoxically, the direct measurement of estradiol and other hormones is not undertaken unless an individual is exhibiting other symptoms of a fertility disorder or hormone imbalance. An implantable, continuously sampling estradiol sensor cannot only help an individual with family planning but can detect if there may be other health risks related to abnormal hormone levels.

For an implantable estradiol sensor to be of clinical use, it must take regular samples and have a lifetime lasting the duration of a menstrual cycle (~30 days). Ideally, the sensor would be able to take a sample every two hours, 360 times. The sensor in its current form should be able to achieve this; however, our experiments testing dissociation capabilities were inconclusive. The sensor should be able to sense a normal estradiol concentration range from approximately 10pmol/L to 1000pmol/L reliably. This means that the sensor must have a limit of detection of at least 10pmol/L, as well as high specificity and selectivity. In its current state, the limit of detection is approximately 36,710pmol/L. Further testing would need to be conducted to quantify the specificity and selectivity of the sensor in its current state.

The sensor is a benchtop setup, taking up approximately $8ft^3$ and powered through a standard wall outlet. To be modified for implantation, the entire sensor would need to be self-contained, and reasonably sized. While an intravaginal ring will likely yield more volume, the device would need to be on the order of mm to be implantable.

The sensor was evaluated in two sets of experiments. The first set of experiments was used to determine if the sensor could differentiate between different levels of estradiol, and the second set of experiments was used to assess the sensor's dissociation capabilities. From the initial experiments, a 3-factor ANOVA determined that although electrode number and day of testing were influential in the reported capacitance, the electrode condition was the most significant parameter in predicting capacitance. The results from the dissociation experiments were inconclusive. Theoretically, the sensor should be able to capture the diurnal estradiol fluctuations, given that the equilibrium dissociation constant is not too low, nor too high.

Thus, the sensor in its current state could be used as a benchtop tool, but many modifications to decrease scale and increase sensitivity would need to be implemented before the sensor is ready for its intended use.

APPENDIX

A ALL CAPACITANCE VALUES

Table A.1: All capacitance values organized by date, electrode condition, and electrode number. Faded cells are omitted trials due to conditions as noted in Section 3.2.6.

Date	**Electrode Condition**	**Electrode Number**	**Capacitance Value [µF/cm^2]**
11.7.21	BG	2	95.95541
11.7.21	BG	3	162.707
11.7.21	BG	4	174.2675
11.29.21	BG	2	26.65924
11.29.21	BG	3	34.40127
11.29.21	BG	4	154.7771
11.7.21	MML	2	4.106688
11.7.21	MML	3	7.452229
11.7.21	MML	4	25.06529
11.9.21	MML	2	5.125159
11.9.21	MML	3	12.47771
11.9.21	MML	4	10.91083
11.16.21	MML	2	4.723567
11.16.21	MML	3	9.856688
11.16.21	MML	4	13.87261
11.23.21	MML	4	18.1051
11.29.21	MML	2	65.31847
11.29.21	MML	3	49.61783

Table A.1 Continued

11.29.21	MML	4	19.81847
11.9.21	E210	2	5.133758
11.9.21	E210	3	10.51274
11.9.21	E210	4	11.17197
11.10.21	E210	2	4.130255
11.10.21	E210	3	10.92357
11.10.21	E210	4	11.95541
11.10.21	E2100	2	5.464968
11.10.21	E2100	3	11.71656
11.10.21	E2100	4	13.03185
11.16.21	E2100	2	4.985987
11.16.21	E2100	3	10.93312
11.16.21	E2100	4	14.13376
11.16.21	E21k	2	4.981529
11.16.21	E21k	3	12.88854
11.16.21	E21k	4	14.53185
11.23.21	E21k	2	11.81529
11.23.21	E21k	3	18.37898
11.23.21	E21k	4	20.47452
11.29.21	E21k	2	14.07643
11.29.21	E21k	3	22.05414
11.29.21	E21k	4	17.24204

APPENDIX

B LIST OF MATERIALS AND MANUFACTURERS

Table B.1: List of materials and their source used for the initial cyclic voltammetry experiments and the dissociation experiments.

Material	**Manufacturer**
Aptamer	University of Utah-HSC Cores
17-β Estradiol	Alfa Aesar
660B Potentiostat	CH Instruments, Inc
Ultrasonic Cleaner 1510	Branson
Vortex-Genie 2 Lab Mixer	GENIE
Thermo Scientific Digital Dry Bath/Block Heater	Fisher Scientific
Standard Gold Electrode	BASi Research Products
Ag/AgCl Electrode	Custom-made
Counter Electrode	Custom-made
Aqueous Electrochemical Cell	Gamry
Felt Polishing Pads	Mirka
1 micron alumina	Kemet
0.3 micron alumina	Kemet
0.05 micron alumina	Kemet

REFERENCES

[1]L. Hariri and A. Rehman, “Estradiol,” *PubMed*, 2022. https://pubmed.ncbi.nlm.nih.gov/31747204/ (accessed Mar. 28, 2022).

[2]“Fertility Awareness,” *Plannedparenthood.org*, 2019. https://www.plannedparenthood.org/learn/birth-control/fertility-awareness.

[3]“What are menstrual irregularities?,” *https://www.nichd.nih.gov/*. https://www.nichd.nih.gov/health/topics/menstruation/conditioninfo/irregularities.

[4]“How every method of hormonal contraception affects your period,” *helloclue.com*. https://helloclue.com/articles/sex/how-every-method-of-hormonal-contraception-affects-your-period.

[5]S. A. Ahmed, B. D. Hissong, D. Verthelyi, K. Donner, K. Becker, and E. Karpuzoglu-Sahin, “Gender and risk of autoimmune diseases: possible role of estrogenic compounds.,” *Environmental Health Perspectives*, vol. 107, no. suppl 5, pp. 681–686, Oct. 1999, doi: 10.1289/ehp.99107s5681.

[6]C.-H. Cheng, L.-R. Chen, and K.-H. Chen, “Osteoporosis Due to Hormone Imbalance: An Overview of the Effects of Estrogen Deficiency and Glucocorticoid Overuse on Bone Turnover,” *International Journal of Molecular Sciences*, vol. 23, no. 3, p. 1376, Jan. 2022, doi: 10.3390/ijms23031376.

[7]M. Lorentzon and S. R. Cummings, “Osteoporosis: the evolution of a diagnosis,” *Journal of Internal Medicine*, vol. 277, no. 6, pp. 650–661, May 2015, doi: 10.1111/joim.12369.

[8]E. Rogan *et al.*, “Relative imbalances in estrogen metabolism and conjugation in breast tissue of women with carcinoma: potential biomarkers of susceptibility to cancer,” *Carcinogenesis*, vol. 24, no. 4, pp. 697–702, Apr. 2003, doi: 10.1093/carcin/bgg004.

[9]D.-R. Chen, W.-C. Hsieh, Y.-L. Liao, K.-J. Lin, Y.-F. Wang, and P.-H. Lin, “Imbalances in the disposition of estrogen and naphthalene in breast cancer patients: a potential biomarker of breast cancer risk,” *Scientific Reports*, vol. 10, no. 1, p. 11773, Jul. 2020, doi: 10.1038/s41598-020-68814-5.

[10]I. J. CHOPRA, “Estrogen-Androgen Imbalance in Hepatic Cirrhosis,” *Annals of Internal Medicine*, vol. 79, no. 2, p. 198, Aug. 1973, doi: 10.7326/0003-4819-79-2-198.

[11]“How is infertility diagnosed?,” *http://www.nichd.nih.gov/*, Jan. 31, 2017. https://www.nichd.nih.gov/health/topics/infertility/conditioninfo/diagnosed.

[12]“5 Myths About Polycystic Ovary Syndrome (PCOS) - Penn Medicine,” *www.pennmedicine.org*, Mar. 18, 2020. https://www.pennmedicine.org/updates/blogs/fertility-blog/2020/march/five-myths-about-pcos#:~:text=Myth%20%233%3A%20PCOS%20is%20a (accessed Mar. 28, 2022).

[13]S. Franks, “Polycystic Ovary Syndrome,” *New England Journal of Medicine*, vol. 333, no. 13, pp. 853–861, Sep. 1995, doi: 10.1056/nejm199509283331307.

[14]L. M. Nelson, “Primary Ovarian Insufficiency,” *The New England journal of medicine*, vol. 360, no. 6, pp. 606–614, Feb. 2009, doi: 10.1056/NEJMcp0808697.

[15]“Rhythm method for natural family planning - Mayo Clinic,” *www.mayoclinic.org*. https://www.mayoclinic.org/tests-procedures/rhythm-method/about/pac-20390918.

[16]“What is the Standard Days Method? | Ovulation Calculator,” *www.plannedparenthood.org*. https://www.plannedparenthood.org/learn/birth-control/fertility-awareness/whats-standard-days-method.

[17]“Clue: Period and Ovulation Tracker for iPhone and Android,” *Helloclue.com*, 2019. https://helloclue.com/.

[18]“How to track your period with Ovia Fertility: The basics,” *Ovia Health*. https://www.oviahealth.com/guide/8/tracking-your-period/ (accessed Mar. 28, 2022).

[19]“GLOW. Ovulation & Period Tracker - Apps on Google Play,” *play.google.com*. https://play.google.com/store/apps/details?id=com.glow.android&hl=en_US&gl=US (accessed Mar. 28, 2022).

[20]“Hormone-Free Birth Control Online,” *Natural Cycles*, Mar. 23, 2020. https://www.naturalcycles.com/.

[21]“Natural family planning (fertility awareness),” *nhs.uk*, Dec. 21, 2017. https://www.nhs.uk/conditions/contraception/natural-family-planning/#:~:text=The%20temperature%20method%20involves%20taking (accessed Mar. 28, 2022).

[22]“Basal body temperature for natural family planning - Mayo Clinic,” *www.mayoclinic.org*. https://www.mayoclinic.org/tests-procedures/basal-body-temperature/about/pac-20393026#:~:text=Basal%20body%20temperature%20may%20increase.

[23]"Cervical mucus method for natural family planning - Mayo Clinic," *www.mayoclinic.org*. https://www.mayoclinic.org/tests-procedures/cervical-mucus-method/about/pac-20393452.

[24]"Estrogen Levels Test: MedlinePlus Lab Test Information," *medlineplus.gov*. https://medlineplus.gov/lab-tests/estrogen-levels-test/.

[25]W. Rosner, S. E. Hankinson, P. M. Sluss, H. W. Vesper, and M. E. Wierman, "Challenges to the Measurement of Estradiol: An Endocrine Society Position Statement," *The Journal of Clinical Endocrinology & Metabolism*, vol. 98, no. 4, pp. 1376–1387, Apr. 2013, doi: 10.1210/jc.2012-3780.

[26]L. Staff, "PreOv is Changing the (Fertility) Game," *Lassonde Entrepreneur Institute – University of Utah*, Apr. 03, 2019. https://lassonde.utah.edu/preov-is-changing-the-fertility-game/ (accessed Mar. 28, 2022).

[27]B. H. Albrecht, R. S. Fernando, J. Regas, and G. Betz, "A new method for predicting and confirming ovulation," *Fertility and Sterility*, vol. 44, no. 2, pp. 200–205, Aug. 1985, doi: 10.1016/S0015-0282(16)48736-4.

[28]B. G. Reed and B. R. Carr, "The Normal Menstrual Cycle and the Control of Ovulation," *Nih.gov*, Aug. 05, 2018. https://www.ncbi.nlm.nih.gov/books/NBK279054/.

[29]"Estrogen and the Menstrual Cycle in Humans | The Embryo Project Encyclopedia," *Asu.edu*, 2016. https://embryo.asu.edu/pages/estrogen-and-menstrual-cycle-humans.

[30]R. Stricker, R. Eberhart, M.-C. Chevailler, F. Quinn, P. Bischof, and R. Stricker, "Establishment of detailed reference values for luteinizing hormone, follicle stimulating hormone, estradiol, and progesterone during different phases of the menstrual cycle on the Abbott ARCHITECT analyzer," *Clinical Chemistry and Laboratory Medicine*, vol. 44, no. 7, pp. 883–887, Sep. 2011, doi: https://doi.org/10.1515/CCLM.2006.160.

[31]L. Ray, "Clue," *Helloclue.com*, 2019. https://helloclue.com/articles/cycle-a-z/the-menstrual-cycle-more-than-just-the-period.

[32]"Can I get pregnant just after my period has finished?," *nhs.uk*, Jun. 27, 2018. https://www.nhs.uk/common-health-questions/pregnancy/can-i-get-pregnant-just-after-my-period-has-finished/#:~:text=You.

[33]B. G. Reed and B. R. Carr, "The Normal Menstrual Cycle and the Control of Ovulation," *Nih.gov*, Aug. 05, 2018. https://www.ncbi.nlm.nih.gov/books/NBK279054/#:~:text=the%20next%20cycle.- (accessed Mar. 28, 2022).

[34]M. M. says, "Estradiol Measurement," *News-Medical.net*, Nov. 15, 2018. https://www.news-medical.net/health/Estradiol-Measurement.aspx.

[35]A.-M. Bao, R.-Y. Liu, E. J. W. van Someren, M. Hofman, Y.-X. Cao, and J.-N. Zhou, "Diurnal rhythm of free estradiol during the menstrual cycle," *European Journal of Endocrinology*, vol. 148, no. 2, pp. 227–232, Feb. 2003, doi: 10.1530/eje.0.1480227.

[36]J. Tachiki-Ryan, "Questions about Layla Wellness, clinical applications, and general fertility.," 2021.

[37]C. Dielen, T. Fiers, S. Somers, E. Deschepper, and J. Gerris, "Correlation between saliva and serum concentrations of estradiol in women undergoing ovarian hyperstimulation with gonadotropins for IVF/ICSI," *Facts, Views & Vision in ObGyn*, vol. 9, no. 2, pp. 85–91, Oct. 2017, Accessed: Mar. 28, 2022. [Online]. Available: https://www.ncbi.nlm.nih.gov/pmc/articles/PMC5707777/.

[38]P. Toniolo *et al.*, "Reliability of measurements of total, protein-bound, and unbound estradiol in serum," *Cancer Epidemiology, Biomarkers & Prevention: A Publication of the American Association for Cancer Research, Cosponsored by the American Society of Preventive Oncology*, vol. 3, no. 1, pp. 47–50, Jan. 1994, Accessed: Mar. 28, 2022. [Online]. Available: https://pubmed.ncbi.nlm.nih.gov/8118385/.

[39]"17B-Estradiol Saliva ELISA," *Ibl-international.com*, 2022. https://www.ibl-international.com/en_us/17beta-estradiol-saliva-elisa (accessed Mar. 28, 2022).

[40]P. Toniolo *et al.*, "Reliability of Measurements of Total, Protein-Bound, and Unbound Estradiol in Serum," *Cancer Epidemiology, Biomarkers & Prevention*, vol. 3, no. 50, pp. 47–50, 1994.

[41]"Nexplanon 68 mg implant for subdermal use - Patient Information Leaflet (PIL) - (emc)," *www.medicines.org.uk*. https://www.medicines.org.uk/emc/product/5720/pil#gref.

[42]"Mobile App User Guide A guide for using the Eversense XL Continuous Glucose Monitoring System Smart Transmitter Sensor." Accessed: Mar. 28, 2022. [Online]. Available: https://global.eversensediabetes.com/sites/default/files/2019-09/LBL-1402-28-001_Rev_B_Eversense_User_Guide_mgdL_UAE_Web.pdf.

[43]"Meet Eversense, the Implantable Continuous Glucose Monitor (CGM)," *Diabetes Daily*, Feb. 07, 2019. https://www.diabetesdaily.com/learn-about-diabetes/technology/tbw-implantables/meet-eversense-the-implantable-continuous-glucose-monitor-cgm/ (accessed Mar. 28, 2022).

[44]H. Elsayed, "Evaluation of Subcutaneous Glucose Monitoring Systems under Routine Environmental Conditions," Medical University of Graz, 2017.

[45]"Comparing Intrauterine Devices (IUD)," University of Michigan Medicine. Accessed: Mar. 28, 2022. [Online]. Available: https://www.med.umich.edu/1libr/Gyn/IUDChart.pdf.

[46]Planned Parenthood, "Planned Parenthood," *Plannedparenthood.org*, 2019. https://www.plannedparenthood.org/learn/birth-control/iud.

[47]"Standardized Procedure: Intrauterine Device/Intrauterine System Insertion (Adult,Peds)," UCSF Medical. [Online]. Available: https://medicalaffairs.ucsf.edu/sites/g/files/tkssra856/f/wysiwyg/ahpPrivileges/IUD%20Insertion%20(Adult,%20Peds).pdf.

[48]"How Is An IUD Inserted?," *Raleigh Gynecology & Wellness*, Sep. 28, 2020. https://gynraleigh.com/how-is-an-iud-inserted/ (accessed Mar. 28, 2022).

[49]"Nuvaring vaginal delivery system - Summary of Product Characteristics (SmPC) - (emc)," *www.medicines.org.uk*. https://www.medicines.org.uk/emc/product/6449/smpc#gref.

[50]"Merck to Dole Out $100 Million in NuvaRing Settlement," *Time*. https://time.com/6515/nuvaring-settlement-100-million-dollars/.

[51]"The Smallest Wireless-Potentiostat｜Zensor R&D｜Potentiostat-ECWP100-single," *www.zensorrd.com*. https://www.zensorrd.com/ECWP100S.html.

[52]D. C. Bock, A. C. Marschilok, K. J. Takeuchi, and E. S. Takeuchi, "Batteries used to power implantable biomedical devices," *Electrochimica Acta*, vol. 84, pp. 155–164, Dec. 2012, doi: 10.1016/j.electacta.2012.03.057.

[53]R. Stoltenburg, C. Reinemann, and B. Strehlitz, "FluMag-SELEX as an advantageous method for DNA aptamer selection," *Analytical and Bioanalytical Chemistry*, vol. 383, no. 1, pp. 83–91, Jul. 2005, doi: 10.1007/s00216-005-3388-9.

[54]B. S. Ferguson *et al.*, "Real-Time, Aptamer-Based Tracking of Circulating Therapeutic Agents in Living Animals," *Science Translational Medicine*, vol. 5, no. 213, Nov. 2013, doi: 10.1126/scitranslmed.3007095.

[55]H. Y. Zheng, O. A. Alsager, C. S. Wood, J. M. Hodgkiss, and N. O. V. Plank, "Carbon nanotube field effect transistor aptasensors for estrogen detection in liquids," *Journal of Vacuum Science & Technology B, Nanotechnology and Microelectronics: Materials, Processing, Measurement, and Phenomena*, vol. 33, no. 6, p. 06F904, Nov. 2015, doi: 10.1116/1.4935246.

[56]J. Li *et al.*, "Sensing Estrogen with Electrochemical Impedance Spectroscopy," *Journal of Analytical Methods in Chemistry*, vol. 2016, p. 9081375, 2016, doi: 10.1155/2016/9081375.

[57]F. V. Oberhaus, D. Frense, and D. Beckmann, “Immobilization Techniques for Aptamers on Gold Electrodes for the Electrochemical Detection of Proteins: A Review,” *Biosensors*, vol. 10, no. 5, p. 45, Apr. 2020, doi: 10.3390/bios10050045.

[58]A. Eisold and D. Labudde, “Detailed Analysis of 17β-Estradiol-Aptamer Interactions: A Molecular Dynamics Simulation Study,” *Molecules (Basel, Switzerland)*, vol. 23, no. 7, p. E1690, Jul. 2018, doi: 10.3390/molecules23071690.

[59]R. Thevendran *et al.*, “Mathematical approaches in estimating aptamer-target binding affinity,” *Analytical Biochemistry*, vol. 600, p. 113742, Jul. 2020, doi: 10.1016/j.ab.2020.113742.

[60]T. M. Herne and M. J. Tarlov, “Characterization of DNA Probes Immobilized on Gold Surfaces,” *Journal of the American Chemical Society*, vol. 119, no. 38, pp. 8916–8920, Sep. 1997, doi: 10.1021/ja9719586.

[61]S. D. Keighley, P. Li, P. Estrela, and P. Migliorato, “Optimization of DNA immobilization on gold electrodes for label-free detection by electrochemical impedance spectroscopy,” *Biosensors and Bioelectronics*, vol. 23, no. 8, pp. 1291–1297, Mar. 2008, doi: 10.1016/j.bios.2007.11.012.

[62]Z. Yang, A. Gonzalez-Cortes, G. Jourquin, J.-C. Viré, J.-M. Kauffmann, and J.-L. Delplancke, “Analytical application of self assembled monolayers on gold electrodes: critical importance of surface pretreatment,” *Biosensors and Bioelectronics*, vol. 10, no. 9, pp. 789–795, Jan. 1995, doi: 10.1016/0956-5663(95)99217-9.

[63]P. Diao, M. Guo, and R. Tong, “Characterization of defects in the formation process of self-assembled thiol monolayers by electrochemical impedance spectroscopy,” *Journal of Electroanalytical Chemistry*, vol. 495, no. 2, pp. 98–105, Jan. 2001, doi: 10.1016/s0022-0728(00)00424-1.

[64]M. M. Ahmadi and G. A. Jullien, “Current-Mirror-Based Potentiostats for Three-Electrode Amperometric Electrochemical Sensors,” *IEEE Transactions on Circuits and Systems I: Regular Papers*, vol. 56, no. 7, pp. 1339–1348, Jul. 2009, doi: 10.1109/TCSI.2008.2005927.

[65]J. Henri, N. Bayat, J. Macdonald, and S. Shigdar, “A guide to using nucleic acid aptamers in cell based assays,” vol. 3, pp. 4–9, 2019, Accessed: Mar. 28, 2022. [Online]. Available: http://japtamers.co.uk/wp-content/uploads/2019/11/Henri.pdf.

[66]Achiko AG and Udayana University, “Saliva-based COVID-19 DNA Aptamer Test: Formative Usability and Internal Validation Study,” *clinicaltrials.gov*, Jul. 21, 2021. https://clinicaltrials.gov/ct2/show/NCT04974203 (accessed Mar. 28, 2022).

[67]Y. Dong, *Aptamers for Analytical Applications : Affinity Acquisition and Method Design*. Weinheim: Wiley-Vch, 2018.

[68]R. L. Rich *et al.*, “Kinetic analysis of estrogen receptor/ligand interactions,” *Proceedings of the National Academy of Sciences*, vol. 99, no. 13, pp. 8562–8567, Jun. 2002, doi: 10.1073/pnas.142288199.

[69]D. G. Myszka, “Improving biosensor analysis,” *Journal of Molecular Recognition*, vol. 12, no. 5, pp. 279–284, Sep. 1999, doi: 3.0.co;2-3">10.1002/(sici)1099-1352(199909/10)12:5<279::aid-jmr473>3.0.co;2-3.